AD-A239 264

ENTATION PAGE

Form Approved
OMB No. 0704-0188

...timated to average 1 hour per response, including the time for reviewing instructions, searching existing data sources, ...ng and reviewing the collection of information. Send comments regarding this burden estimate or any other aspect of this ... burden, to Washington Headquarters Services, Directorate for Information Operations and Reports, 1215 Jefferson Davis Highway, Suite 1204, Arlington, VA 22202-4302, and to the Office of Management and Budget, Paperwork Reduction Project (0704-0188), Washington, DC 20503.

1. AGENCY USE ONLY (Leave blank)	2. REPORT DATE	3. REPORT TYPE AND DATES COVERED
		FINAL 01 Aug 88 to 30 Sep 90

4. TITLE AND SUBTITLE
COHERENCE AND CHAOS IN INTEGRABLE PDEs (PARTIAL DIFFERENTIAL EQUATIONS)

5. FUNDING NUMBERS
AFOSR-88-0195
61102F/2304/K7

6. AUTHOR(S)
EDWARD OVERMAN

7. PERFORMING ORGANIZATION NAME(S) AND ADDRESS(ES)
OHIO STATE UNIVERISTY
DEPARTMENT OF MATHEMATICS
1314 KINNEAR ROAD
COLUMBUS OH 43212-1994

8. PERFORMING ORGANIZATION REPORT NUMBER
AFOSR-TR- 91. 0694
AFOSR-88-0195

9. SPONSORING/MONITORING AGENCY NAME(S) AND ADDRESS(ES)
AFOSR/NM
Bldg 410
Bolling AFB DC 20332-6448

10. SPONSORING/MONITORING AGENCY REPORT NUMBER

11. SUPPLEMENTARY NOTES

DTIC
ELECTE
AUG 09 1991
S D
D

12a. DISTRIBUTION/AVAILABILITY STATEMENT
Approved for public release;
distribution unlimited.

12b. DISTRIBUTION CODE

13. ABSTRACT (Maximum 200 words)

The results of the efforts for grant AFOSR-88-0195 are:
1) numerically identified low dimensional chaotic attractors with spatially coherent structures:
2) measured the preperties of the chaos:
3) identified the sources and types of chaos:
4) determined natural coordinates for the attractor which are associated with the simple spatial patterns in chaos:
5) used these coordinates to calculate reduced systems of equations which have the same routes to chaos and qualitatively-and quatitatively-similar strange attractors.

91-07419

14. SUBJECT TERMS

15. NUMBER OF PAGES

16. PRICE CODE

17. SECURITY CLASSIFICATION OF REPORT	18. SECURITY CLASSIFICATION OF THIS PAGE	19. SECURITY CLASSIFICATION OF ABSTRACT	20. LIMITATION OF ABSTRACT
UNCLASSIFIED	UNCLASSIFIED	UNCLASSIFIED	SAR

THE OHIO STATE UNIVERSITY

Coherence and Chaos in Integrable PDEs (Partial Differential Equations)

Edward A. Overman
Department of Mathematics

Air Force Office of Scientific Research
Bolling Air Force Base, D.C. 20332-6448

Grant No. AFOSR-88-0195
Final Report
RF Project No. 766917/721140

Accession For
NTIS CRA&I
DTIC TAB
Unannounced
Justification
By
Distribution /
Availability Codes
Dist | Avail and/or Special
A-1

March 1991

In the last seven years there has been a large group effort devoted to studying chaos and coherence in "near" integrable pdes. The group of Alan Bishop of the Los Alamos National Laboratory, Nick Ercolani of the University of Arizona, David McLaughlin of Princeton University, and Greg Forest, Amar Sinha, and the author of the Ohio State University have been studying perturbed sine-Gordon and nonlinear Schrödinger equations. Our efforts have been concentrated in the following areas:

(1) numerically identifying low dimensional chaotic attractors with spatially coherent structures;
(2) measuring the properties of the chaos;
(3) identifying the sources and types of chaos;
(4) determining natural coordinates for the attractor which are associated with the simple spatial patterns in chaos;
(5) and using these coordinates to calculate reduced systems of equations which have the same routes to chaos and qualitatively — and quantitatively — similar strange attractors.

This study, as with most other such studies [1,2,3,4,5], has relied heavily on numeric. computations — even with the rich structure of completely integrable systems. However, because of this rich structure we have been able to use numerical experimentation to gain insight into the analytical behavior of the system; this has not generally been true in the pde literature (see, for example [6,7,8,9]).

For certain parameter regimes of the sine-Gordon and the nonlinear Schrödinger equations we have made large gains in the first four areas and are now concentrating on the fifth. From numerical experiments [10] it is clear that soliton waveforms are natural candidates for the coordinates of the attractor and that only a very small number of these modes are sufficient. The soliton perturbation theory of the 1970's [11,12,13] is inadequate to dress this calculation of reduced systems since this perturbation theory has great difficu.. in handling the transitions between the various spectral coordinates (kink, breather, and radiation).

Instead we are exploiting the rich geometric structure in phase space of these integrable Hamiltonian systems. The geometry of this infinite dimensional phase space — with its separatices and homoclinic orbits — enables us to identify precisely the sources of chaos, to determine the number of nonlinear modes required, and to identify the transitions between the various nonlinear modes [14,15]. Thus, nearby integrability provides sufficient control to yield very precise and detailed information about the structure of the chaotic attractors — much more detailed information than can be anticipated for general pdes.

Of course, the final goal of this lengthy study is to able to study chaos in more general systems in one and more space dimensions. For example, our analytical and numerical results on homoclinic orbits should be applicable to a large class of systems where this seems to be the origin of the chaos. And our work on natural coordinates for the attractor (i.e., global and local bases in chaos) should be applicable in systems where the localized solutions are not known analytically. At present we are using what is known about chaos in more general systems simply as a guide to the areas we should be concentrating on. In the near future we expect to actually apply our results to some of these systems where we will have to rely almost totally on numerical computations, techniques, and results.

Let me be specific on our results to date in the following areas:

(a) sample numerical results,
(b) data analysis,
(c) homoclinic orbits as sources of chaos,
(d) geometry of the integrable sine-gordon equation,
(e) reduced system of odes,
(f) similarity between the chaos in the full and reduced systems, and
(g) an analytic study of these homoclinic orbits.

We have been studying the driven, damped sine-Gordon equation with periodic boundary conditions:

$$u_{xx} - u_{tt} = \sin u + \epsilon\,(\alpha u_t - \Gamma \cos \omega t) \tag{1}$$

$$u(x+L,t) = u(x,t), \quad u(x,t=0) = u_{in}(x), \quad u_t(x,t=0) = v_{in}(x). \tag{1a}$$

Here ϵ is a small positive parameter, $\alpha > 0$ measures the strength of dissipation. the amplitude of the sinusoidal driver and ω is its frequency, and L is the spatial pe:.. The initial data $u_{in}(x)$ is periodic with period L and has one maximum in this period. The initial data $v_{in}(x)$ is usually 0. (In almost all the experiments we have studied to date the initial data is symmetric and so the waveform remains symmetric for all time.)

In Josephson junctions, which consists of two superconducting metal layers separated by a thin insulating oxide layer, which is small enough to permit quantum-mechanical tunnelling of electrons, different perturbations are generally used [16,17,18]] and so we are now studying

$$u_{xx} - u_{tt} = \sin u + \epsilon\,(\alpha u_t - \beta u_{xxt} - \Gamma \cos \omega t + \gamma).$$

This adds a dc driver energy source and a dissipation which depends on the wavenumber.

(a) **Sample Numerical Results.** We have been studying eq. (1) numerically as described in [10,19]. By varying ϵ, α, Γ, ω, and L we have found several robust attractors with distinct routes to chaos (see also [5,20]). The parameter values we are concentrating on are $L = 12$, $\epsilon\alpha = 0.04$, $\omega = 0.87$, and we use the amplitude of the sinusoidal driver as the stress parameter ($0.0 < \epsilon\Gamma < 0.15$). Our route to chaos is (see Fig. 1 for plots of these regions):

$\epsilon\Gamma \lesssim 0.050$ —
spatially flat – temporally locked to the driver (Fig. 1a);

$0.050 \lesssim \epsilon\Gamma \lesssim 0.058$ —
spatially one excitation – temporally locked to the driver (Figs. 1b and 1c);

$\epsilon\Gamma \approx 0.058$ —
spatially one excitation – quasiperiodic in time (Fig. 1d);

$\epsilon\Gamma \approx 0.0585$ —
spatially one excitation – temporally chaotic (this is a very small region which may simply be a result of our numerical code — see Fig. 1e), the corresponding energy of the solution as a function of time is shown in Fig. 1f;

$0.059 \lesssim \epsilon\Gamma \lesssim 0.073$ —
spatially flat – temporally locked to the driver (Fig. 1g), there seem to be some very

small windows of one spatial excitation and quasi-periodicity in time which are not shown;

$0.073 \lesssim \epsilon\Gamma$ —

spatially one excitation – temporally chaotic (Fig. 1h).

Numerically the spatial state seems to consist of a chaotic visiting of three states—a breather localized in the center, a breather localized in the wings, and a flat state. In addition, the waveform is low amplitude (~ 2) and seems to consist of two nonlinear modes—a breather and $m = 0$ radiation, and $m = 1$ and $m = 0$ radiation (i.e., $\cos 2\pi m x/L$). We emphasize that this chaotic motion occurs for $\epsilon\Gamma \approx 0.07$, a value at which the system is still near the integrable sine-Gordon equation.

This parameter region has been chosen because the chaos is very simple and the reduced system of equations does a good job of explaining our results. The details will be discussed below and unless otherwise noted all discussion and plots will correspond to this parameter region.

There are two other parameter regions that are very important. The first is the same as the above except that $L = 24$. The route to chaos is similar but the chaos itself is more complicated [10]. That is, there is a chaotic bouncing between one spatial excitation and two spatial excitations per period. In addition, if symmetry is not imposed on the pde then there is a translational instability in the waveform.

In the other parameter regime there is a very unusual period-doubling route to chaos. This is where $L = 80$, $\epsilon\alpha = 0.004$, and $\omega = 0.98$. The route to chaos (as Γ increases) goes from spatially flat to spatially one excitation and from periodic to quasiperiodic in time [21]. However in this quasiperiodicity there is a period doubling into chaos! That is, when we do a Poincare map to factor out the phase of the driver then we see a period doubling into chaos. (First there is just one point, corresponding to the periodic Then there is a closed curve, corresponding to the quasi-periodic orbit. Then this closed curve goes unstable and becomes a closed curve which crosses itself, etc.) Then, as above, as Γ is increased further only the flat wave remains stable, and finally chaos reappears.

It is our belief that all three parameter regimes arise from the same cause — namely homoclinic orbits. As will be described below we have verified this (to our satisfaction) in the first region, we see no reason to doubt it in the second region, and it seems reasonable in the third region but much work remains to be done.

(b) **Data Analysis.** In order to establish the structure of these attractors we have used standard diagnostics to analyze our numerical data. In particular the temporal behavior is analyzed with standard diagnostics from dynamical systems theory, such as time series, phase planes, Poincare sections, temporal power spectra, leading Lyapunov exponents, and correlation dimensions. All temporal diagnostics are consistent with the above description of the attractors.

In addition we are studying the local behavior of the orthonormal basis which is used to construct the Lyapunov exponents. To explain this let us begin with how Lyapunov exponents are calculated both analytically and numerically [22].

Let our system, $\dot{\vec{x}} = \vec{f}(x,t)$ be N dimensional and consider a trajectory $\{\vec{x}(t) | t \geq 0\}$ where $\vec{x}(0) = \vec{x}_0$. Along with this trajectory consider the evolution of the volume consisting of all the initial conditions that lie within an infinitesimal ball of radius ϵ

centered at $\vec{x}_0$. The evolution of this ball is an ellipsoid (since its evolution is determined by the linear part of the flow) with principal axes of length $\epsilon_i(t)$ where $\epsilon_i(0) = \epsilon$ for $1 \leq i \leq N$. Then the Lyapunov exponents, λ_i, are defined by

$$\lambda_i = \lim_{t\to\infty} \lim_{\epsilon\to 0} \frac{\epsilon_i(t)}{\epsilon}$$

where $\lambda_1 \geq \lambda_2 \geq \ldots$.

Numerically, however, we pick a time Δt and integrate an orthonormal basis (which represents this ball) forward in time by Δt *using the linearized equations.* We then re-orthonormalize by using a Gram-Schmidt procedure to find the lengths of these principal axes and repeat this procedure for K time intervals. If we let the length of the i^{th} principal axis at the end of the k^{th} time interval be $\delta x^i(k)$ (where $\epsilon = 1$) then

$$\lambda_i = \lim_{K\to\infty} \frac{1}{K\Delta t} \sum_{k=1}^{K} \ln \delta x^i(k) \tag{3a}$$

Instead of studying the Lyapunov exponent we study

$$\sum_{k=k_0}^{k_1} \ln \delta x^i(k) \tag{3b}$$

directly as a function of $(k-k_0)\Delta t$. (We call these the local Lyapunov exponents — lLe's.) The reason for our choice can be seen in Figs. 2. In Fig. 2a we show the convergence $(\ln \delta x^1(k))/\Delta t$ as a function of $k\Delta t$. There is one positive Lyapunov exponent, two zero Lyapunov exponents (if symmetry is used in the code then there is only one), and the other five Lyapunov exponents (that were calculated) have the same negative value. In Fig. 2b we plot $\sum_k \ln \delta x^1(k)$ as a function of $(k-k_0)\Delta t$ where the quasiperiodic-like character of the chaos can be easily seen. Note that this repeated signature — of length ~ 50 corresponds to the random fluctuations of the breather-like waveform (as in Fig. 1h) as the waveform dies out and then recovers either as before or shifted by $L/2$. Thus the average length of these signatures gives the time for this recovery — although it does not indicate whether the new breather-like waveform is shifted with respect to the old or not. In addition, the occasional huge jumps in this local Lyapunov exponent are caused by the flat waveform persisting for a much longer period of time. In the ode systems this corresponds to the trajectory circling around an unstable fixed point for a few rotations before zooming off again. In Fig. 2c we again plot $\sum_k \ln \delta x^1(k)$ as a function of $(k-k_0)\Delta t$ but for the 6 dimensional sine-Gordon ode. At least to the naked eye these curves are very similar — even to having the same huge jumps.

There are many advantages to studying these local Lyapunov exponents:

1) These lLe's are functions of time and so can exhibit much interesting behavior over the whole trajectory as opposed to the Lyapunov exponents which are a time average over the whole trajectory.

2) These lLe's are ordered so that the leading one or ones show the exponential rate of separation which is the characteristic of chaos. In fact for the sine-Gordon pde and for our particular parameter regime $\lambda_1 > 0$, $\lambda_2 = \lambda_3 = 0$, and $\lambda_4 = \lambda_5 = \ldots = \lambda_8 < 0$ (which is all the Lyapunov exponents we have calculated since each one takes as long to solve as the original pde). The first lLe (shown in Fig. 2b) and the second and third ones have the same characteristic signature and look quite similar (although their slopes are quite different). The remaining lLe's all look similar to the lLe's for non-chaotic waveforms.
3) These lLe's give an overall picture of the trajectory as opposed, for example, to plots of the j^{th} component of the trajectory.
4) We can study statistical properties of these lLe's and so compare chaotic trajectories between the sine-Gordon pde, the nonlinear Schrödinger pde, the sine-Gordon odes, and the nonlinear Schrödinger odes. This includes studying correlations, power spectra, etc. in order to determine quantitative measures of the differences between different trajectories.

The spatial behavior is analyzed with the inverse scattering transform which measures quantitatively both the soliton and radiation nonlinear modes that comprise the attractor at a given time [19]. With $L = 12$ we find that the number of appreciably excited nonlinear modes is 2 at the onset of chaos and increases slowly with increasing $\epsilon\Gamma$. The chaotic attractor itself can be described by these modes undergoing collision, annihilation, nucleation, and energy transfer between coherent (localized) states and radiation (extended) states. These transitions involve what we call the "crossing of homoclinic states" and are shown in Figs. 3. Notice how the spectrum (the wiggly line) oscillates between a cross (for example at $t = 25{,}036$) and a gap (for example at $t = 25{,}048$). The homoclinic orbit corresponds to the spectral configuration between these two times where the gap closes and the two pieces of spectrum just touch. As time evolves these two pieces of spectrum merge into one and push the spectrum out (approximately) perpendicular to the cross indicated by the dots (this is discussed in detail in [27]). The gap configuration always corresponds to higher energy and to a more focused waveform (i.e., more localized).

(c) **Homoclinic Orbits as Sources of Chaos.** Often the origin of chaos, and of its associated sensitivity, can be traced to homoclinic orbits of a nearby integrable system. This source of chaos is well understood in odes. For example, in the damped, driven pendulum the unperturbed, infinite period separatrix is a homoclinic orbit. The motion of the pendulum near its inverted position is extremely sensitive to the sinusoidal driver. Thus, small perturbations can cause the pendulum to either return to its original potential well or to be kicked into the next potential well. Random and chaotic behavior results as a consequence of this sensitivity [23]. In the pde case detailed geometric information about infinite dimensional phase space is generally not available. However, for the special integrable pdes of soliton theory such geometric information is becoming available. For the Korteweg-de Vries equation under periodic boundary conditions a rather complete geometric theory exists [24]. It is interesting to note that this periodic KdV system has no homoclinic orbits, no instabilities, and no separatices—and requires very strong stresses to become chaotic. On the other hand the periodic sine-Gordon equation possesses a much richer geometric structure [25] than KdV. The sine-Gordon equation has many homoclinic

states throughout its phase space whichprovide a source of chaos when the system is driven; and, indeed, the chaotic structure is very rich.

Homoclinic orbits can occur whenever the spectrum has a critical point [15]. That is, the spectrum is all the values of λ where an analytical function called the discriminant, $\Delta(\lambda)$, is real and $-2 \leq \Delta \leq +2$. A critical point λ_c is wherever $\Delta(\lambda_c) = \pm 2$ and $\Delta'(\lambda_c) = 0$. If a critical point satisfies $\Re(\lambda_c) > 0$ and $\Im(\lambda_c) > 0$ then it can have exponential growth [15]. We have explicitly calculated the homoclinic orbit which seems to be the source of the chaos. It is shown in Fig. 4a and a representative plot of the chaotic trajectory from Fig. 1h is shown in Fig. 4b. As a more accurate comparison we plot $u(x = 0, t)$ for both the homoclinic orbit and the chaotic trajectory in Fig. 4c.

Thus, the nonlinear transform has established that unperturbed homoclinic states, which are potential sources of sensitivity, are indeed present. We emphasize that this explicit and precise identification of the homoclinic states and their crossings is only possible because we are in a near integrable situation and have a precise tool (the nonl transform) for their detection.

(d) **Geometry of the Integrable Sine-Gordon Equation** This theoretical work [14,15] may be summarized geometrically as an extension of the 2-dimensional phase portrait for the pendulum into the infinite dimensional phase space of the integrable periodic sine-Gordon equation, and physically as an extension of the classical description of a long wavelength, linear instability of trivial solutions to both a linear and a global description of similar instabilities for arbitrary N-phase solutions. It is this basic theory that has enabled us to detect—with the nonlinear spectral measuring device—the presence of homoclin crossings in the numerical data for the chaotic attractor.

The theoretical understanding we have obtained about the Benjamin-Feir unstable modes has given an analytical underpinning to the numerical calculations of the presence of homoclinic orbits in the chaotic waveforms. Additionally we have been able to explicitly write down the homoclinic orbit which seems to be the cause of the chaos in the parameter region with $L = 12$ as described above. (This solution is no easy feat since it involves the Jacobi eta, theta, and zeta functions!)

(e) **Reduced System of Odes.** Since the geometry of the sine-Gordon phase space is quite complicated [14,15], we have constructed reduced systems of odes to approximate the infinite dimensional pde using both Fourier modes and Lumley modes [26]. (Lumley modes are orthogonal, coherent modes in chaos which are "best" in some least-squares sense). Preliminary work has begun by Forest, McLaughlin, and Sinha on expanding the waveform in a nonlinear basis (using the geometry of the sine-Gordon phase space). Early results are promising. However our work will continue to focus on linear bases.

Three reduced systems have been studied in great detail. The first is a reduced system of ordinary differential equations directly taken from the sine-Gordon pde. That is, we assume

$$u(x,t) = \sum_{k=0}^{\infty} a_k(t) e_k(x) \qquad (4)$$

and truncate this linear combination to solve the $2N^{\text{th}}$ order sine-Gordon ode system

$$\ddot{a}_k = a_k\langle e_k'', e_k\rangle - \left\langle \sin(\sum_{k=0}^{N-1} a_k e_k), e_k \right\rangle - \epsilon\alpha\dot{a}_k + \epsilon\Gamma \sin\omega t \,\langle 1, e_k\rangle \tag{5}$$

for $k = 0, 1, 2, \ldots, N-1$. There are two possibilities here: 1) leave the problem as it is and calculate the inner product containing the sine term at each time step; or 2) expand the sine term into the first two or three terms of its Taylor series so that this inner product can be calculated once and for all. The second approach has the virtue of saving a significant amount of computer time. The first approach has the advantage of being more accurate and allowing any number of basis functions to see if some sort of convergence is obtained as $N \to \infty$. We are using both approaches. We are also using two different choices for the e_k's, namely, cosine modes and Lumley modes.

The second is to derive a perturbed nonlinear Schrödinger envelope equation from e (1). Letting

$$\begin{aligned} &\omega = 1 - \epsilon\tilde{\omega}, \quad \epsilon\alpha = 2\tilde{\omega}\tilde{\alpha}, \quad \epsilon\Gamma = 8\sqrt{\epsilon\tilde{\omega}}\,\tilde{\omega}\tilde{\Gamma}, \quad \tilde{L} = \sqrt{2\epsilon\tilde{\omega}}L, \\ &X = \sqrt{2\epsilon\tilde{\omega}}x, \quad T = \epsilon\tilde{\omega}t, \quad u(x,t) = 2\sqrt{\epsilon\tilde{\omega}}\,[B(X,T)\exp^{i\omega t} + c.c.] + O(\epsilon) \end{aligned} \tag{6}$$

and keeping the first two terms in the Taylor series expansion for $\sin u$, then the slowly varying envelope $B(X,T)$ satisfies

$$-iB_T + B_{XX} + (|B|^2 - 1)B = i\tilde{\alpha}B - \tilde{\Gamma}. \tag{7}$$

We have achieved two things by this reduction. First, we have preserved the pertur integrable structure since the unperturbed pde of eq. (7) (i.e., $\tilde{\alpha} = \tilde{\Gamma} = 0$) is the integrable nonlinear Schrödinger equation. Second, we have factored out the frequency of the driver, ω. Thus, periodic solutions of the sine-Gordon equation correspond to fixed points of the nonlinear Schrödinger equation, quasiperiodic solutions of the sine-Gordon equation correspond to periodic solutions, which are incommensurate with ω, of the nonlinear Schrödinger equation, and chaotic solutions of the sine-Gordon equation correspond to chaotic solutions of the nonlinear Schrödinger equation.

We now make a further approximation and truncation based on the numerically observed low number of nonlinear modes, namely

$$B(X,T) = \sum_{k=0}^{N-1} A_k(t)\cos\tilde{k}X \tag{8}$$

(where the A's are complex). We then obtain an explicit system of ordinary differential equations in A_k using Mathematica. At present we have used $N \leq 5$.

In particular, for $N = 2$ we obtain the 4^{th}–order system of odes

$$\begin{aligned} -ic_T + (|c|^2 + \frac{1}{2}|b|^2 - 1)c + \frac{1}{2}(c\bar{b} + \bar{c}b)b &= i\tilde{\alpha}c - \tilde{\Gamma}, \\ -ib_T + (|c|^2 + \frac{3}{4}|b|^2 - [1 + \tilde{k}^2])b + (c\bar{b} + \bar{c}b)c &= i\tilde{\alpha}b \end{aligned} \tag{9}$$

which is, in fact, an integrable Hamiltonian system [27]. Its constants of the motion are

$$I = |c|^2 + \frac{1}{2}|b|^2,$$
$$H = \frac{1}{2}|c|^4 + |b|^2|c|^2 + \frac{3}{16}|b|^4 - \frac{1}{2}(1+\tilde{k}^2)|b|^2 - |c|^2 + \frac{1}{4}(b^2\bar{c}^2 + \bar{b}^2c^2). \tag{10}$$

The fixed points of the ode correspond qualitatively to the periodic solutions of the pde before the onset of chaos; and, in chaos, the three unstable fixed points of the ode which seem to be the basis for the attractor correspond in the pde to a breather localized in the center, a breather localized in the wings, and a flat state (see Fig. 1h). In addition, the homoclinic crossings of the pde correspond quite accurately to the zeroes of

$$h = H - (\frac{1}{2}I^2 - I). \tag{11}$$

Although this ode truncation cannot be expected to yield quantitative agreement with the pde it does model most of the apparent features of the route into chaos and the behavior in chaos of the pde. This is somewhat surprising since the approximations necessary to obtain eq. (7) require replacing $\sin u$ by $u - u^3/6$ (even though $max\{u\} > 2$) and neglecting the next term in the expansion in ϵ, namely $O(\sqrt{\epsilon})$.

(f) **Similarity Between the Chaos in the Full and Reduced Systems.** To verify that the chaos in the full sine-Gordon pde and in various lower order truncations are *similar* we need to show that the strange attractor is *similar* in some sense. As discussed abc method to determine the similarity between two chaotic trajectories is to compare local Lyapunov exponents. This comparison is shown in Figs. 2b and 2c. To make t... comparison more qualitative we have taken the power spectra of these two figures and plot them in Figs. 5. We are presently working with Mark Berliner of the Statistics Department in trying to determine how precisely we can say that two chaotic trajectories are "similar". This includes studying correlations, power spectra, etc. in order to determine quantitative measures of the differences between different trajectors. Our main emphasis is using the lLe's since these give a basis free view of the strange attractor. At present we can say that certain trajectories are "closer" than others but we still need to develop a technique for calculating error bounds so that we can show that two trajectories, corresponding to the same parameters but different initial conditions, are "very similar". In this way we could check whether, for example, chaotic trajectories in the sine-Gordon odes converge to chaotic trajectories in the sine-Gordon pde as we increase their dimension. (They certainly *seem* to be "close".) In this way we could show (at least numerically) that the geometry underlying the sine-Gordon odes is the cause of the chaos in the sine-Gordon pde.

As a second measure of the similarities between the various systems we are using the bifurcation sequences of the various ode truncations which we are calculating using a public domain bifurcation package AUTO [28] as well as a bifurcation code written by Xiong to provide backup support for AUTO for verification, to use in place of AUTO when AUTO seems not to be working correctly, and to study in more detail the structure of this bifurcation sequence. In Figs. 6a and 6b we compare the bifurcation sequence for the

6^{th}−order nonlinear Scorödinger ode and the 6^{th}−order sine-Gordon ode respectively. We cannot follow the Hopf bifurcation in the sine-Gordon ode since it corresponds to a quasi-periodic orbit, but otherwise the two sequences are very similar. (The norms (the vertical axes) are not the same in both plots and so the curves look different — but the critical points all occur at approximately the same values of $\epsilon\Gamma$). In particular, as the order of the sine-Gordon ode increases the critical points seem to approach the boundaries of the sine-Gordon pde. Even for the 6^{th}−order ode the accuracy is to within $\sim 10\%$ for all the critical points shown. In particular, whereas the 4^{th}−order ode has a subcritical Hopf bifurcation (and so does the 4^{th}−order nls ode) all higher order systems have a supercritical Hopf bifurcation which corresponds to the quasi-periodicity in the pde at $\epsilon\Gamma \sim 0.058$. Also, the extent (in Γ) of these quasi-periodic solution agrees very well with the range found numerically in the pde. Thus we are fully confident that the geometry underlying the ode systems can explain the transition to chaos in the pde.

(g) **An analytic study of these homoclinic orbits.** Dave McLaughlin and Steve Wiggins are working with Chuyu Xiong and me in attempting to use singular perturbation theory to understand the nature of the homoclinic orbits which are the sources of the chaos. This work is still preliminary but Xiong and I are developing better numerical techniques to study periodic orbits which are very close to the homoclinic orbit. (We have not been able to develop any techniques to solve for the homoclinic orbit directly since the fixed point corresponding to this homoclinic orbit is 2-dimensionally unstable.) With our numerical results they are able to determine how to do their perturbation expansions.

Publications

Two papers have arisen so far from this study. In the first [29] we did an analytical and numerical perturbation analysis on the nonlinear Schrödinger equation for $\epsilon\alpha = 0.04$, $L = 12$ and $L = 24$, and for various ω and Γ. This entailed calculating the waveform in a perturbation expansion and using this in stability calculations. This allowed us to validate the solutions we were seeing numerically in the pde and to obtain our first bifurcation sequence (similar to Figs. 6) for comparison. It also allowed us to understand how the bifurcation sequence changes as α and ω vary. However this paper was concerned strictly with the physical plane and never made use of the spectral transformation underlying the sine-Gordon pde (i.e., the underlying geometry of the pde).

In the second paper [27] the first attempt was made to study the geometry of the pde explicitly. In this study we attempted to understand the transition to chaos for the parameter regime $L = 12$. $\epsilon\alpha = 0.04$, and $\omega = 0.87$ (although the analysis is certainly applicable for other regimes). This was done by studying the 4^{th}−order nonlinear Schrödinger equation, eq. (9) ode both numerically and analytically. The unperturbed system is completely integrable and so has a well-understood geometric structure. We were able to show that the stable fixed points of the perturbed system corresponded to the flat and periodic solutions of the sine-Gordon pde. We were also able to show that the chaos in the ode arose from the fixed points corresponding to these periodic solutions becoming unstable. Finally we could identify a homoclinic orbit in the sine-Gordon pde with a function of the two constants of motion in the ode system and thus construct the homoclinic orbit we believed to be the source of the chaos explicitly for the ode. We could

then show that this ode homoclinic orbit was crossed repeatedly in chaos. Of course, this study was carried out in a *very* low dimensional ode and so it was certainly not obvious that the chaos in the pde could be understood by this simplified model (and we made that point in the paper).

At present we are writing up our results in comparing the sine-Gordon pde with all of the various truncations discussed above. This will leave no doubt that, in fact, the geometry of the low dimensional ode truncations (as long as they are at least $6^{th}-$order) is sufficient to explain the chaos in the pde by showing the convergence to the limit of the sine-Gordon odes to the sine-Gordon pde [30]. Additionally it will demonstrate new methods for showing the "closeness" between various strange attractors which will allow us to quickly determine the similarity between the chaotic responses of various systems.

Finally we are writing up our work on the explicit calculation of the homoclinic orbit which seems to be the cause of the chaos in the pde [31]. This will include a discussion of the various solutions that arise from one and two Bäcklund transformations of the McCumber solution (i.e., spatially flat) and their stability. Both breather-like (i.e., symmetric) and kink-like (i.e., asymmetric) waveforms will be studied.

Invited Talks

Invited talks on these subjects were given at:

- Conference on Nonlinear Transport Properties in Condensed Matter Physics, July, 1989, at the Technical University of Denmark.
- IMACS International Conference on Computational Physics, June 1990, at the University of Colorado.

Figure Captions

1. Numerically computed solutions of the perturbed sine-Gordon equation for $L = 12$, $\epsilon\alpha = 0.04$, $\omega = 0.87$ and for various values of $\epsilon\Gamma$. (a) $\epsilon\Gamma = 0.48$, (b) $\epsilon\Gamma = 0.50$, (c) $\epsilon\Gamma = 0.57$, (d) $\epsilon\Gamma = 0.58$, (e) $\epsilon\Gamma = 0.586$, (f) the energy as a function of time for the waveform shown in (e) to make the evolution clearer (also shown are the l_2 averages in x of u and u_t as a function of time), (g) $\epsilon\Gamma = 0.72$, and (h) $\epsilon\Gamma = 0.75$.

2. Plots of the leading Lyapunov exponents for the run with parameters $L = 12$, $\epsilon\alpha = 0.04$, $\epsilon\Gamma = 0.075$, and $\omega = 0.87$. (a) The Lyapunov exponents are the limiting values of these curves (i.e., as $t \to \infty$). (b) The local Lyapunov exponent for the the sine-Gordon pde. (c) The local Lyapunov exponent for the 6 dimensional sine-Gordon ode.

3. Spectra for the run with parameters $L = 12$, $\epsilon\alpha = 0.04$, $\epsilon\Gamma = 0.075$, and $\omega = 0.87$. Some crosses and gapes are noted in the plots. (a) The sine-Gordon spectra at various times. (b) The plot of $u(x,t)$ as a function of t corresponding to the times of the spectra.

4. (a) The homoclinic orbit which appears to be the source of the chaos for the run shown in Fig. 1h. (b) An enlarged view of the chaotic trajectory to the same scale as (a). (c) A comparison of the homoclinic orbit with the chaotic trajectory by plotting $u(x = 0, t)$ for each (the solid line is the homoclinic orbit and the dashed line is the chaotic trajectory).

5. Power spectra of the leading local Lyapunov exponent corresponding to the same runs as in Fig. 2. (a) The pde; (b) the ode.

6. Bifurcation sequence for the 6^{th}–order nonlinear Schrödinger ode (a) and the 6^{th}–order sine-Gordon ode (b). (The norms, i.e., the vertical axes, are not the same in both plots and so the curves look different — but the critical points all occur at approximately the same values of $\epsilon\Gamma$. Also the horizontal axes are not to the same scale)

7. The time evolution (a) and the corresponding spectrum (b) for $L = 80$, $\epsilon\alpha = 0.004$, $\epsilon\Gamma = 0.0043$, and $\omega = 0.87$.

8. (a) The time evolution of a solution to the exact nonlinear Schrödinger pde using 24 points. (b) The time evolution of the spectrum during the time that the solution begins to move. At each time the top two plots show the waveform as its magnitude, phase, real part, and imaginary part. The main plot shows the spectrum. The spectrum is the solid lines along with the horizontal axis ('G' means the spectrum is in a gap configuration, 'C' means it is in a cross configuration, and 'S' means the spectrum has split asymmetrically). The small crosses are where the discriminant is real but less than -2 and the small pluses are where the discriminant is real but greather than $+2$. The bottom plot shows the values of the discriminant on the real axis.

References

1. *Spatial-Temporal Coherence and Chaos in Physical Systems*, edited by Alan R. Bishop, G. Gruner, and Basil Nicolaenko, Physica **23D** (1986).
2. *Order in Chaos*, edited by David Campbell and Harvey Rose, Physica **7D** (1983).
3. *Solitons and Coherent Structures*, edited by David Campbell, Alan C. Newell, R. Schrieffer, and Harvey Segur, Physica **18D** (1986).
4. *Nonlinear Systems of Partial Differential Equations, Parts 1 and 2; Lectures in Appl. Math.* **23**, edited by Basil Nicolaenko, Darrel Holm, and and J. Mac Hyman (American Mathematical Society, Providence, Rhode Island, 1986).
5. H. T. Moon, Patrick Huerre, and L. G. Redekopp, *Transitions to Chaos in the Ginzburg-Landau Equation*, Physica **7D**, 135 (1983);
   L. R. Keefe, *Dynamics of Perturbed Wavetrain Solutions to the Ginzburg-Landau Equation*, Studies in App. Math. **73**, 91 (1985).
6. K. Nozaki and N. Bekki, *Chaos in a Perturbed NLS Equation*, Phys. Rev. Lett. **50**, 1226 (1984);
   K. Nozaki and N. Bekki, *Solitons as Attractors of a Forced, Dissipative NLS Equation*, Phys. Lett. **102A**, 383 (1984);
   K. Nozaki and N. Bekki, *Low Dimensional chaos in a Driven, Damped NLS Equation*, Physica **21D**, 381 (1986).
7. H. H. Chen, Y. C. Lee, and E. Tracy, *Study of Quasi-Periodic Solutions of the [illegible] Equation and the Nonlinear Modulational Instability*, Phys. Rev. Lett. **53**, 218
8. Y. C. Lee and H. H. Chen, *Nonlinear Dynamical Models of Plasma Turbulence*, Physica Scrita **T2**, 41 (1982).
9. B. Birnir, *Chaotic Perburtations of KdV Equations*, Physica **18D**, 464 (1986);
   B. Birnir, *Chaotic Solutions of KdV I: Rational Solutions*, Physica **19D**, 238 (1986).
10. Alan R. Bishop, M. Greg Forest, David W. McLaughlin, and Edward A. Overman II, *A Quasi-Periodic Route to Chaos in a Near Integrable PDE*, Physica **23D**, 293–329 (1986);
    Alan R. Bishop, M. Greg Forest, David W. McLaughlin, and Edward A. Overman II, *A Quasi-Periodic Route to Chaos in a Near-Integrable Pde: Homoclinic Crossings*, Phys. Lett. A. **127**, 335–340 (1988).
11. David J. Kaup and Alan C. Newell, *Solitons as Particles and Oscillators: A Singular Perturbation Theory*, Proc. Roy. Soc. Lond. **A361**, 413 (1978).
12. David W. McLaughlin and Alwyn C. Scott, *Perturbation Analysis of Fluxon Dynamics*, Phys. Rev. **A18**, 1652 (1978).
13. Mark J. Ablowitz and Yuji Kodama, *Perturbation of Solitons and Solitary Waves*, Stud. Appl. Math. **64**, 226 (1981).
14. Nick Ercolani, M. Greg Forest, and David W. McLaughlin, *Modulational Instabilities of Periodic Sine-Gordon Waves: A Geometric Analysis*, Lectures in Appl. Math. **23**,

149 (1986);
Nick Ercolani, M. Greg Forest, and David W. McLaughlin, *The Origin and Saturation of Modulational Instabilities*, Physica **18D**, 472 (1986).

15. Nick Ercolani, M. Greg Forest, and David W. McLaughlin, *Geometry of the Modulational Instability. Part I: Local Analysis*; to appear in Memoirs of the AMS;
Nick Ercolani, M. Greg Forest, and David W. McLaughlin, *Geometry of the Modulational Instability. Part II: Global Analysis*; to appear in Memoirs of the AMS;
Nick Ercolani, M. Greg Forest, and David W. McLaughlin, *Homoclinic Orbits for the Periodic sine-Gordon Equation*, Physica **43D**, 349–384 (1990).

16. B. D. Josephson, *Suppercurrents through Barriers*, Advances in Phys. **14**, 419–451 (1965);
Alwyn C. Scott, *Profpagation of Magnetic Flux on a Long Josephson Tunnel Junction*, Nuovo Cimento B **13**, 241–260 (1970).

17. Antonio Barone and Gianfranco Paternò, *Physics and Applications of the Josephs Effect*, John Wiley & Sons (New York, 1982).

18. L. E. Guerrero and M. Octavio, *Quasiperiodic and Chaotic Behavior Due to Competition between Spatial and Temporal Modes in Long Josephson Junctions*, Phys. Rev. A **37**, 3641–3644 (1988);
Sergio Pagano, Mads P. Sörenson, Peter L. Christiansen, and Robert D. Parmentier, *Stability of Fluxon Motion in Long Josephson Junctions at High Bias*, Phys. Rev. B **38** (1988).

19. Edward A. Overman II, David W. McLaughlin, and Alan R. Bishop, *Coherence Chaos in the Driven, Damped Sine-Gordon Equation: Measurement of the Soliton Spectrum*, Physica **19D**, 1 (1986).

20. D. Bennett, Alan R. Bishop, and Steven E. Trullinger, *Coherence and Chaos in the Driven Damped Sine-Gordon Equation*, Z. Phys. **B47**, 165 (1982);
Alan R. Bishop, Klaus Fesser, Peter S. Lomdahl, William C. Kerr, M. B. Williams, and Steven E. Trullinger, *Coherent Spatial Structure Versus Time Chaos in a Perturbed Sine-Gordon System*, Phys. Rev. Lett. **50**, 1095 (1983);
Alan R. Bishop, Klaus Fesser, Peter S. Lomdahl, and Steven E. Trullinger, *Influence of Solitons in the Initial State on Chaos in the Driven, Damped Sine-Gordon Equation*, Physica **7D**, 259 (1983);
J. C. Eilbeck, Peter S. Lomdahl, and Alan C. Newell, *Chaos in the Inhomogeneously Driven Sine-Gordon Equation*, Phys. Lett. **87A**, 259 (1981).

21. Magid Taki and K. H. Spatschek, *Temporal Chaos via Period-doubling Route in Sine-Gordon System*; to appear in Journal de Physique, Paris.

22. J. Doyne Farmer, *Chaotic Attractors of an Infinite-Dimensional Dynamical System*, Physica **4D**, 366–393 (1982).

23. J. Guckenheimer and Philip Holmes, *Nonlinear Oscillations. Dynamical Systems, and Bifurcations of Vector Fields*, Springer (New York, 1983).

24. H. P. McKean and E. Trubowitz, *Hill's Operator and Hyperelliptic Function Theory in the Presence of Infinitely Many Branch Points*, Comm. Pure Appl. Math. **29**, 143 (1976);
H. P. McKean, *Stability for the Korteweg-de Vries Equation*, Comm. Pure Appl. Math. **30**, 347 (1977).

25. H. P. McKean, *The Sine-Gordon and Sinh-Gordon Equations on the Circle*, Comm. Pure Appl. Math. **34**, 197 (1981).

26. D. J. L. Lumley, *Coherent Structures in Turbulence*, in: *Transition and Turbulence*, edited by R. E. Meyer (Academic Press, New York, 1981).

27. Alan R. Bishop, Randy Flesch, M. Greg Forest, David W. McLaughlin, and Edward A. Overman II, *Correlations Between Chaos in a Perturbed Sine-Gordon Equation and a Truncated Model System*, SIAM J. of App. Math. **21**, 1511–1536 (1990).

28. E. J. Doedel, *AUTO, A Program for the Automatic Bifurcation Analysis of Autonomous Systems*, Cong. Num. **30**, 265–284 (1981) (Proc. 10th Manitoba Conf. on Num. Math. and Comp., Univ. of Manitoba, Winnipeg, Canada (1980)).

29. Guillermo Terrones, David W. McLaughlin, Edward A. Overman II, and Arne J. Pearlstein, *Stability and Bifurcation of Spatially Coherent Solutions of the Damped-driven NLS Equation*, SIAM J. App. Math. **50**, 791–818 (1990).

30. Edward A. Overman II, Chuyu Xiong, and Mark Berliner, *Convergence of Low-Mode Truncations of the Driven Damped Sine-Gordon Equation* (in preparation).

31. M. Greg Forest, Edward A. Overman II, Peter Christiansen, Randy Flesch, and David W. McLaughlin, *A Homoclinic Orbit in the Periodic Sine-Gordon Equation* (in ration).

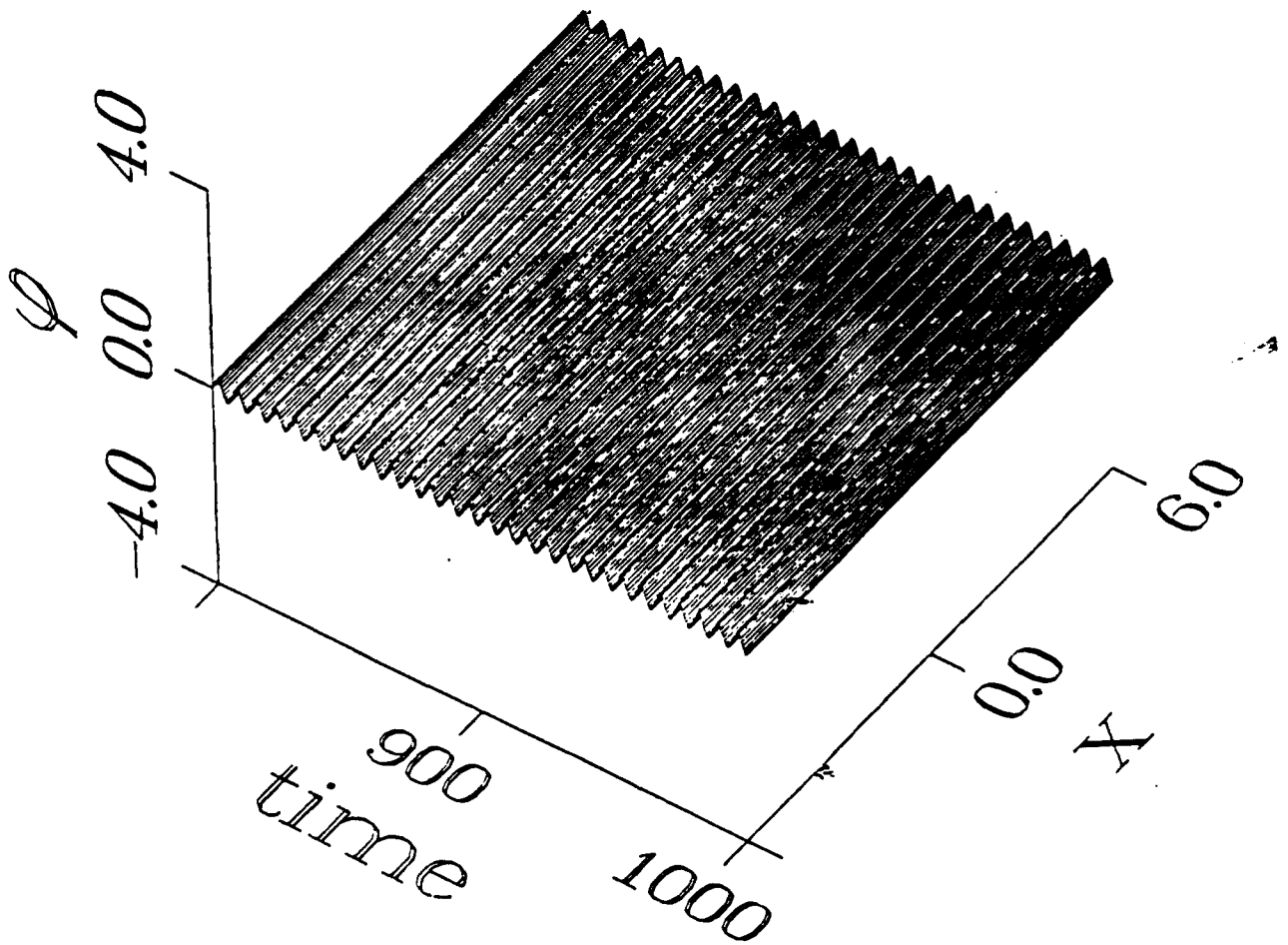

Figure 1 (a)

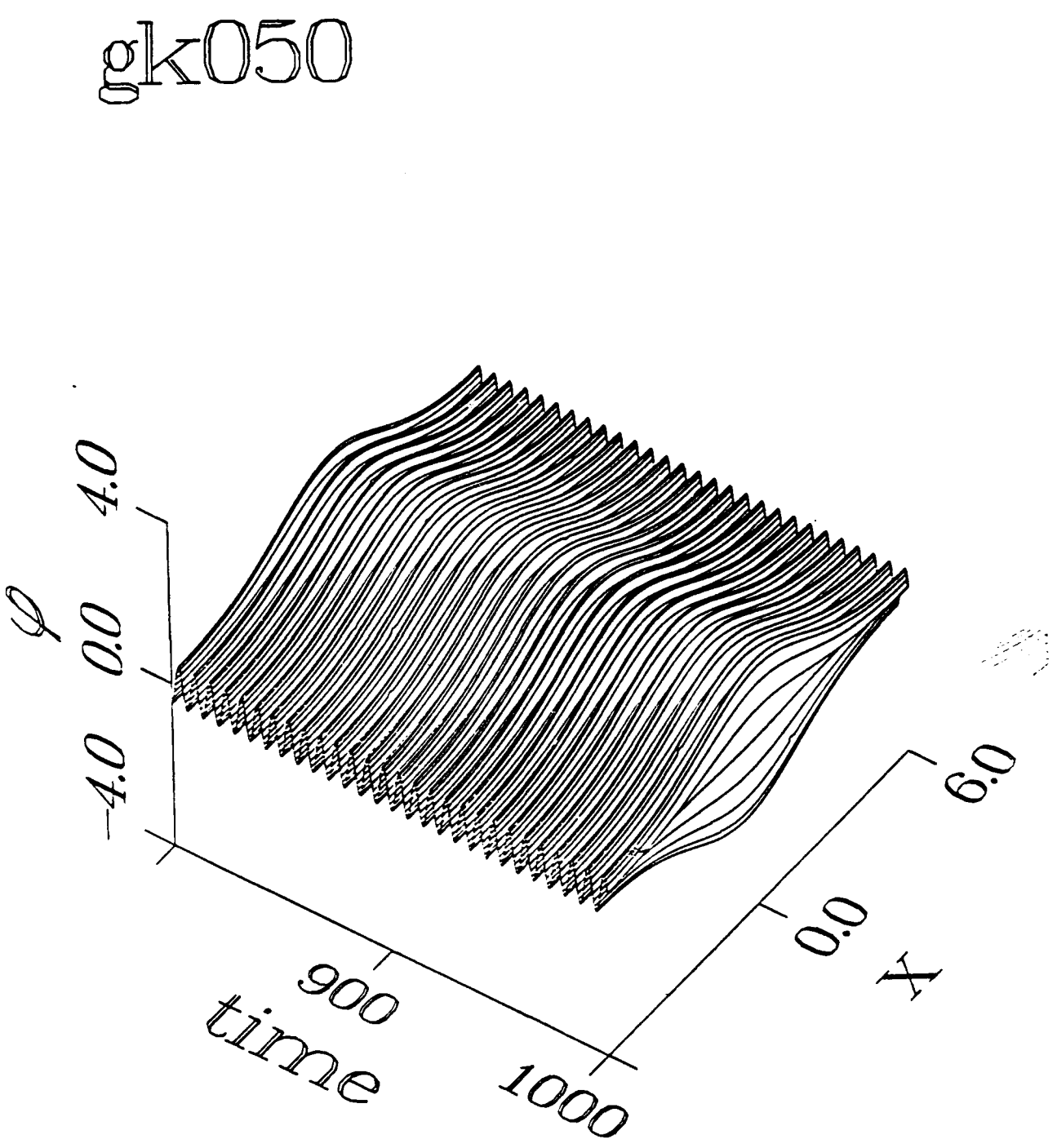

Figure 1 (b)

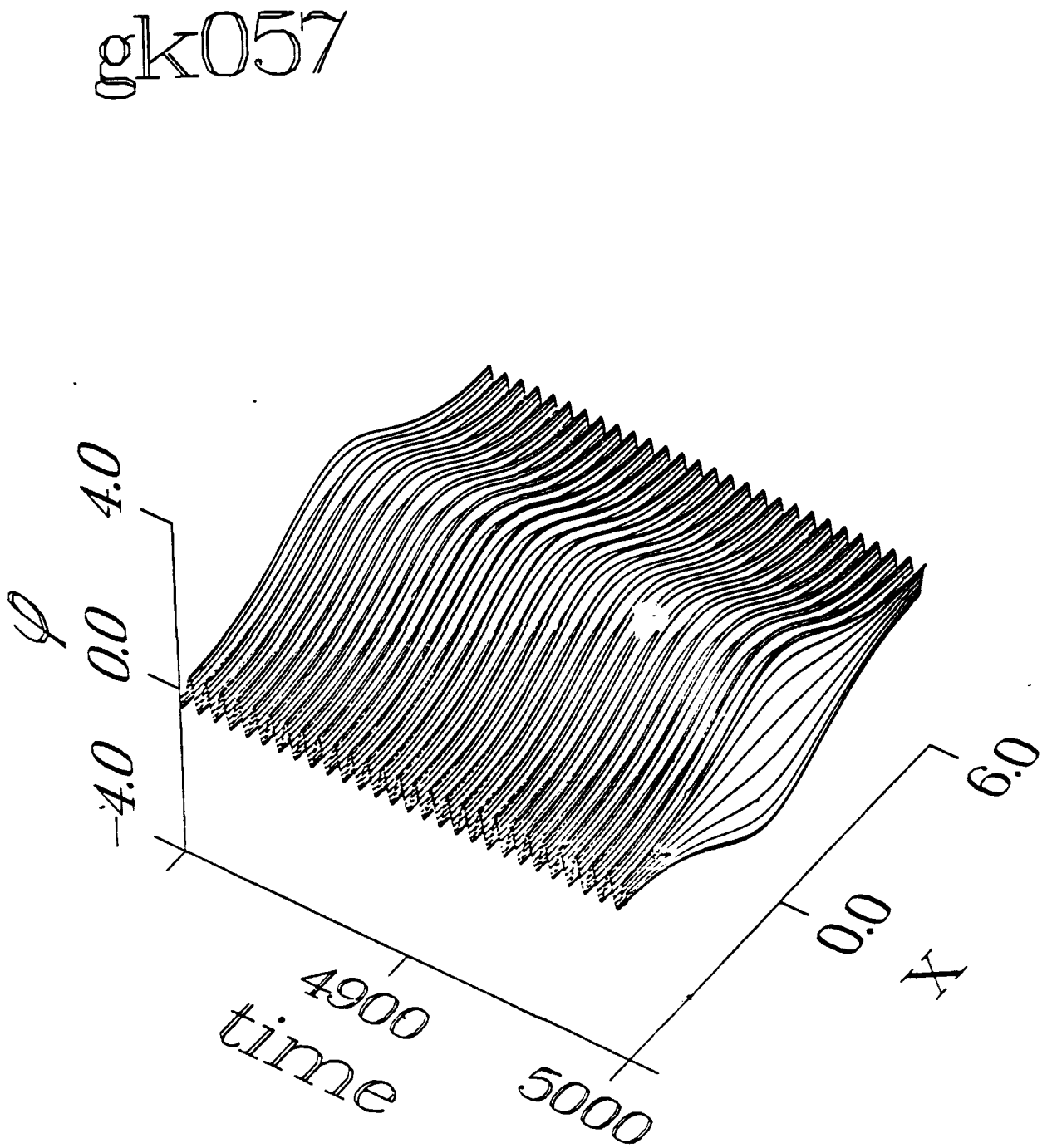

Figure 1 (c)

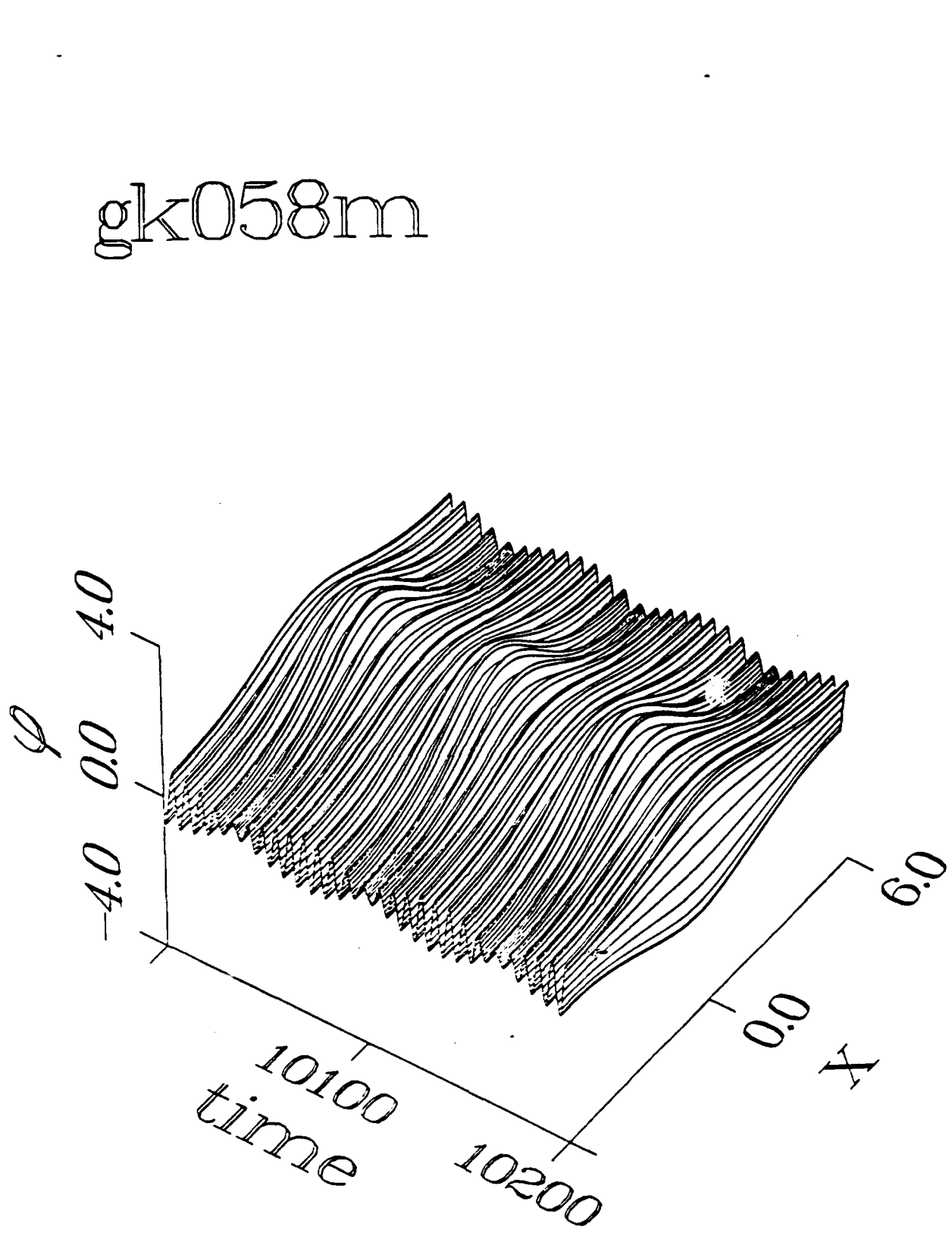

Figure 1 (d)

gk0586m

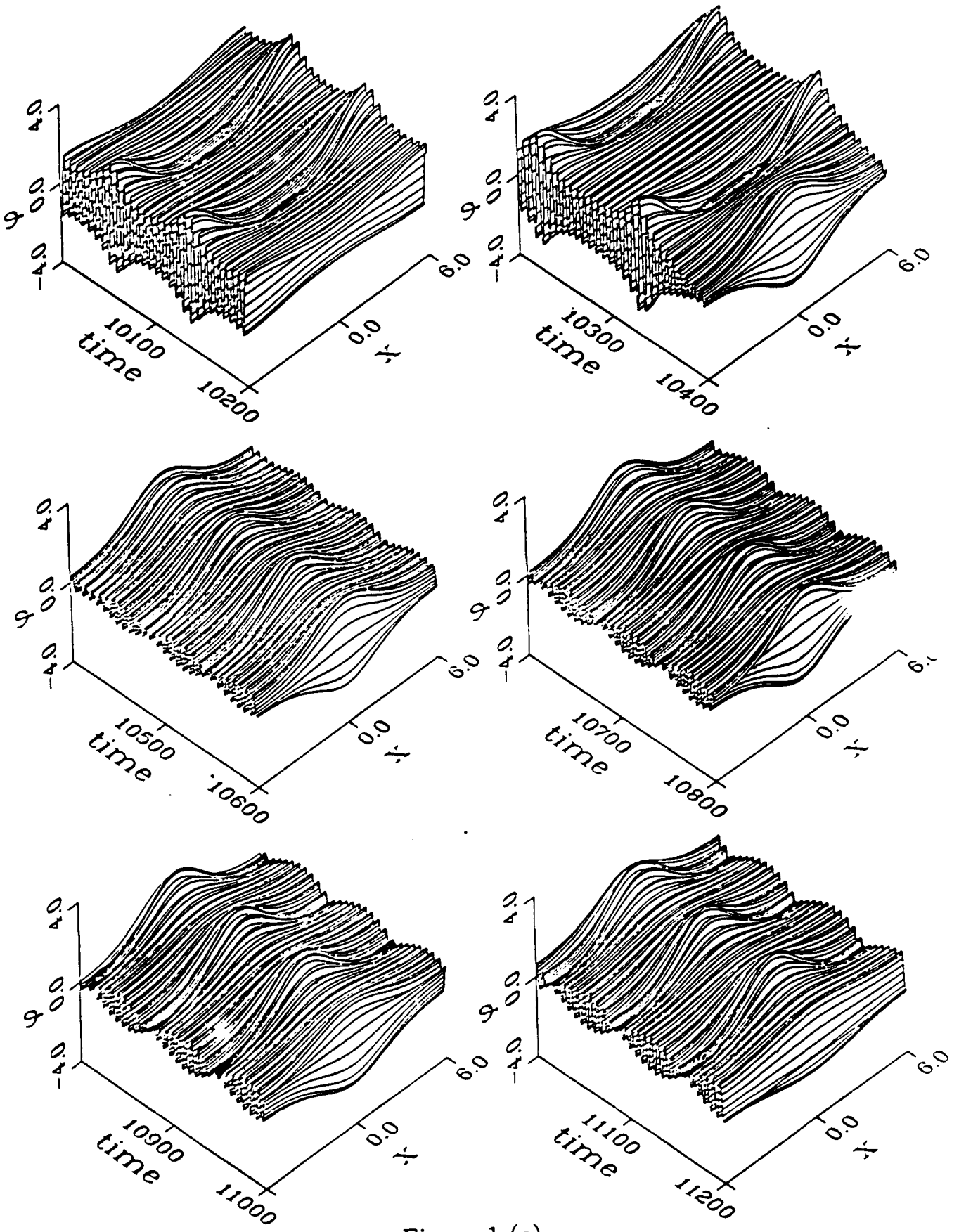

Figure 1 (e)

gk0586m

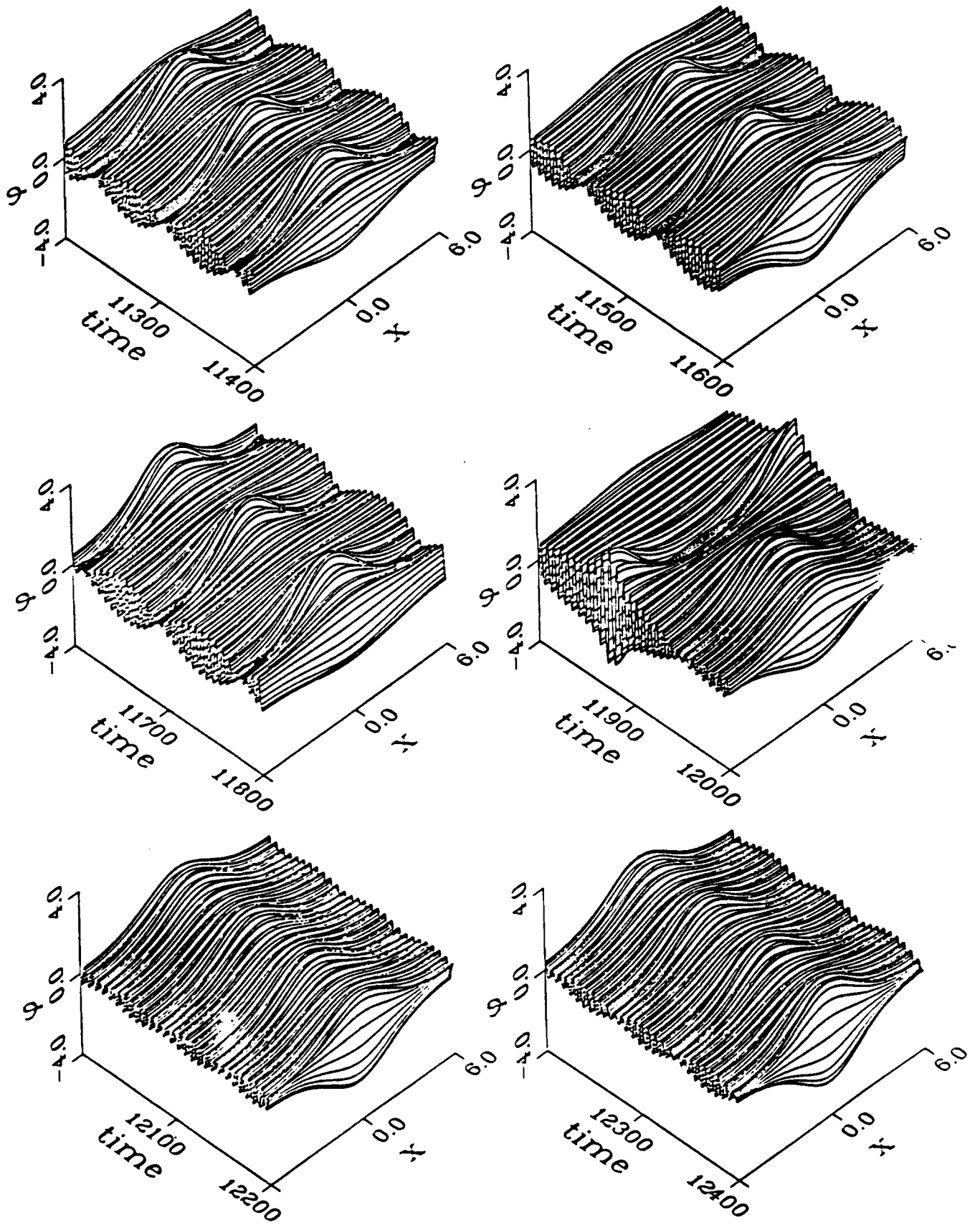
0.4
0.0
-0.4
φ
11300
time
11400
0.0
x
6.0
11500
11600
11700
11800
11900
12000
12100
12200
12300
12400

gk0586m

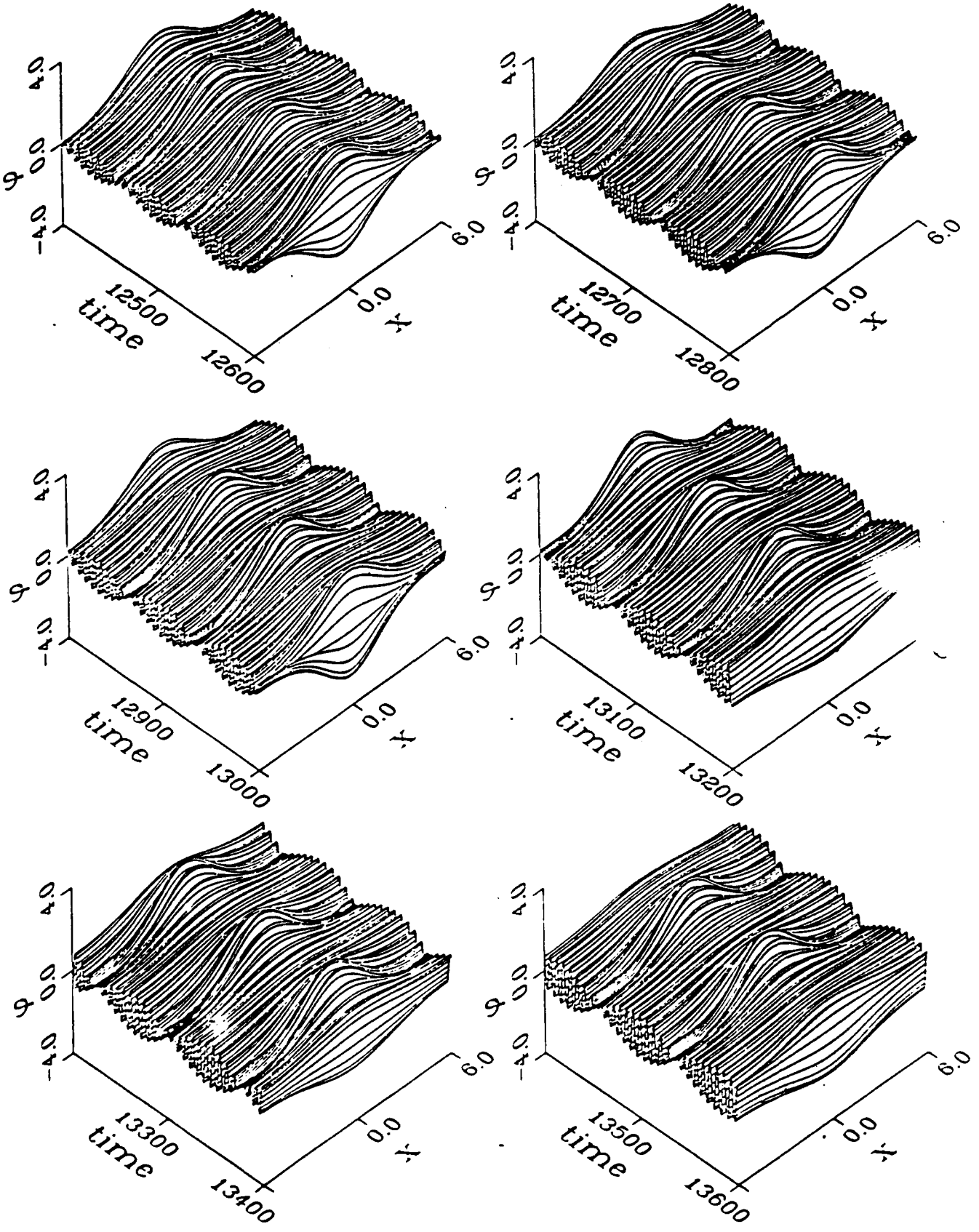
0.4
0.0
-0.4
φ
12500
time
12600
0.0
x
6.0
12700
12800
12900
13000
13100
13200
13300
13400
13500
13600

gk0586m

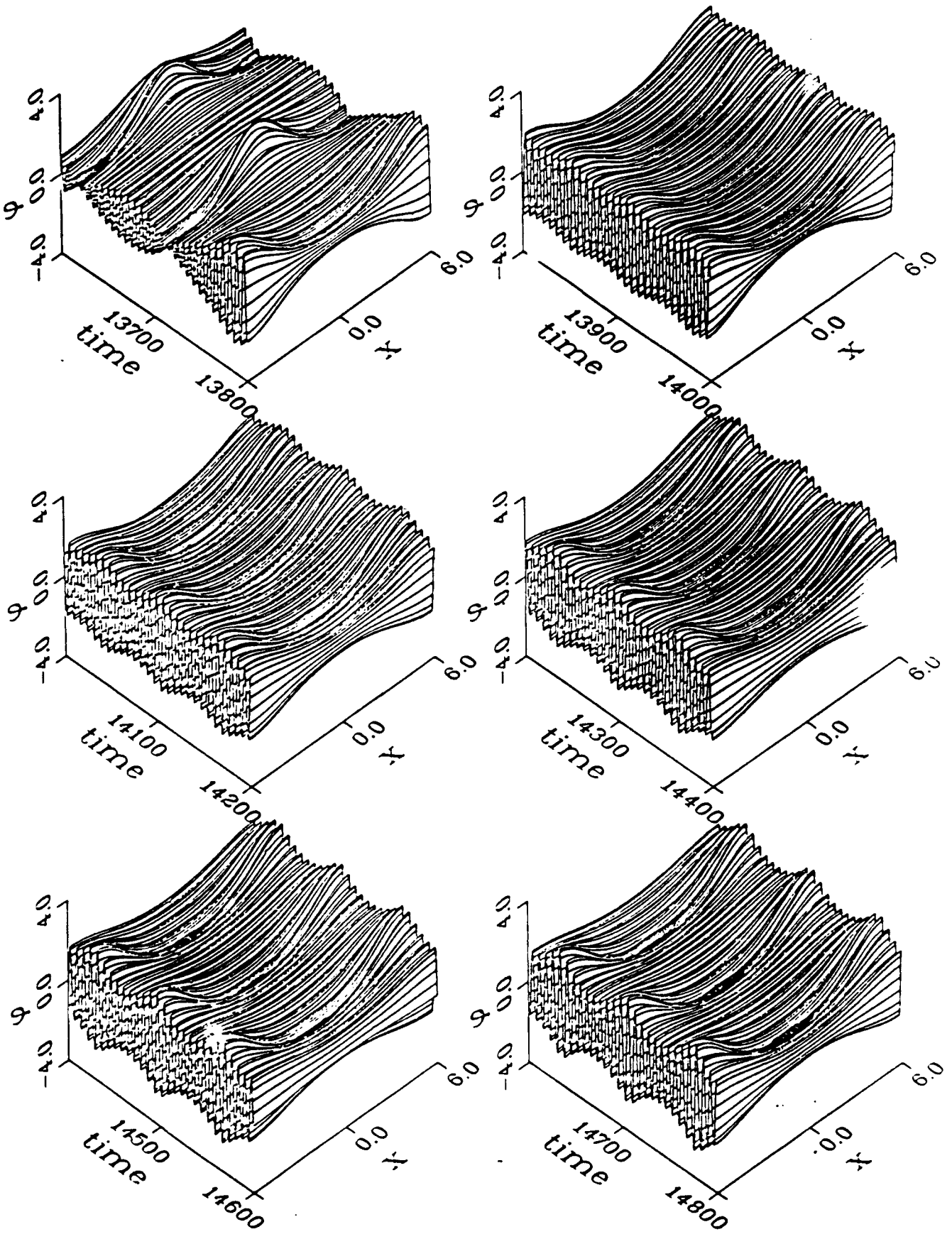
0.4
0.0
-0.4
θ
13700
time
13800
0.0
x
6.0
13900
14000
14100
14200
14300
14400
14500
14600
14700
14800

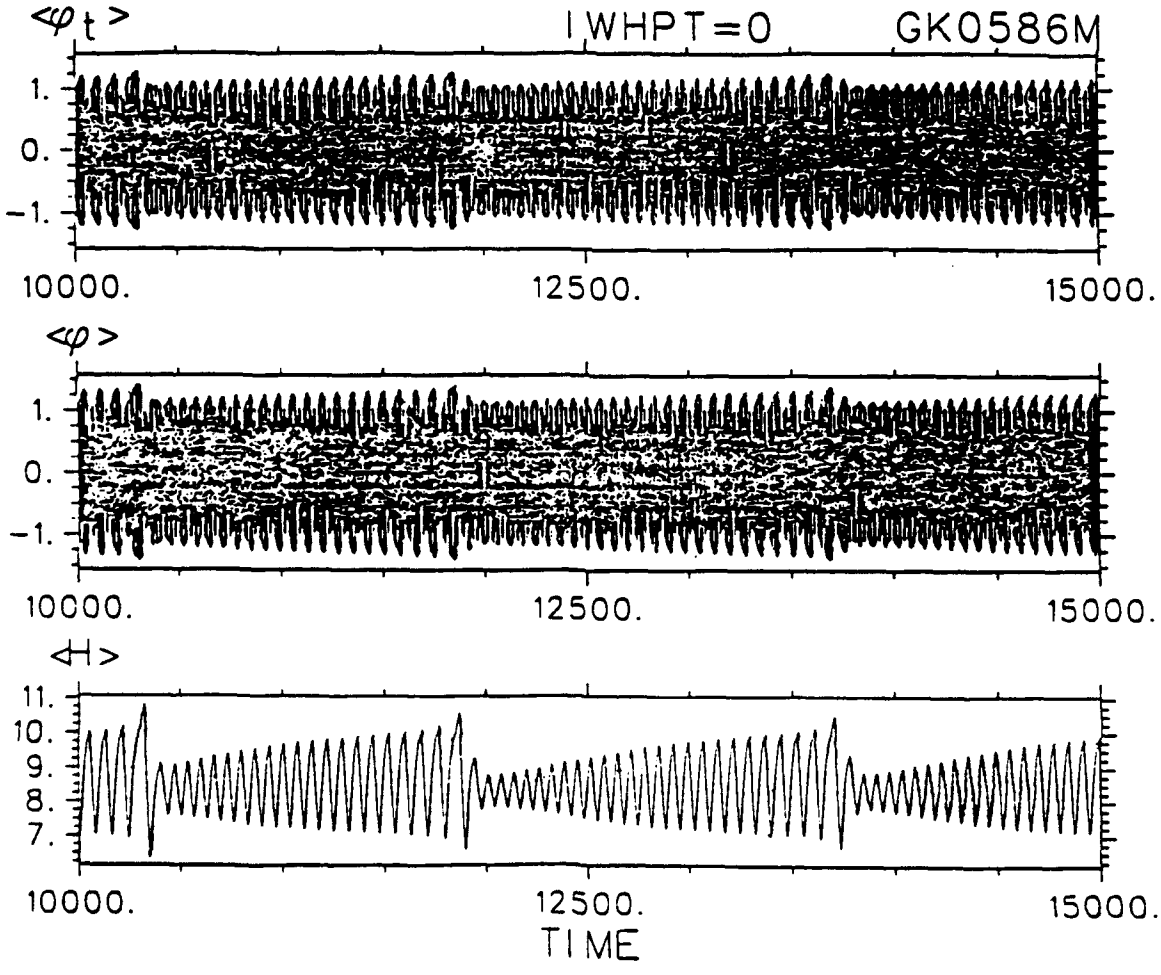
<φt>
IWHPT=0
GK0586M
1.
0.
-1.
10000.
12500.
15000.
<φ>
1.
0.
-1.
10000.
12500.
15000.
<H>
11.
10.
9.
8.
7.
10000.
12500.
15000.
TIME

Figure 1 (f)

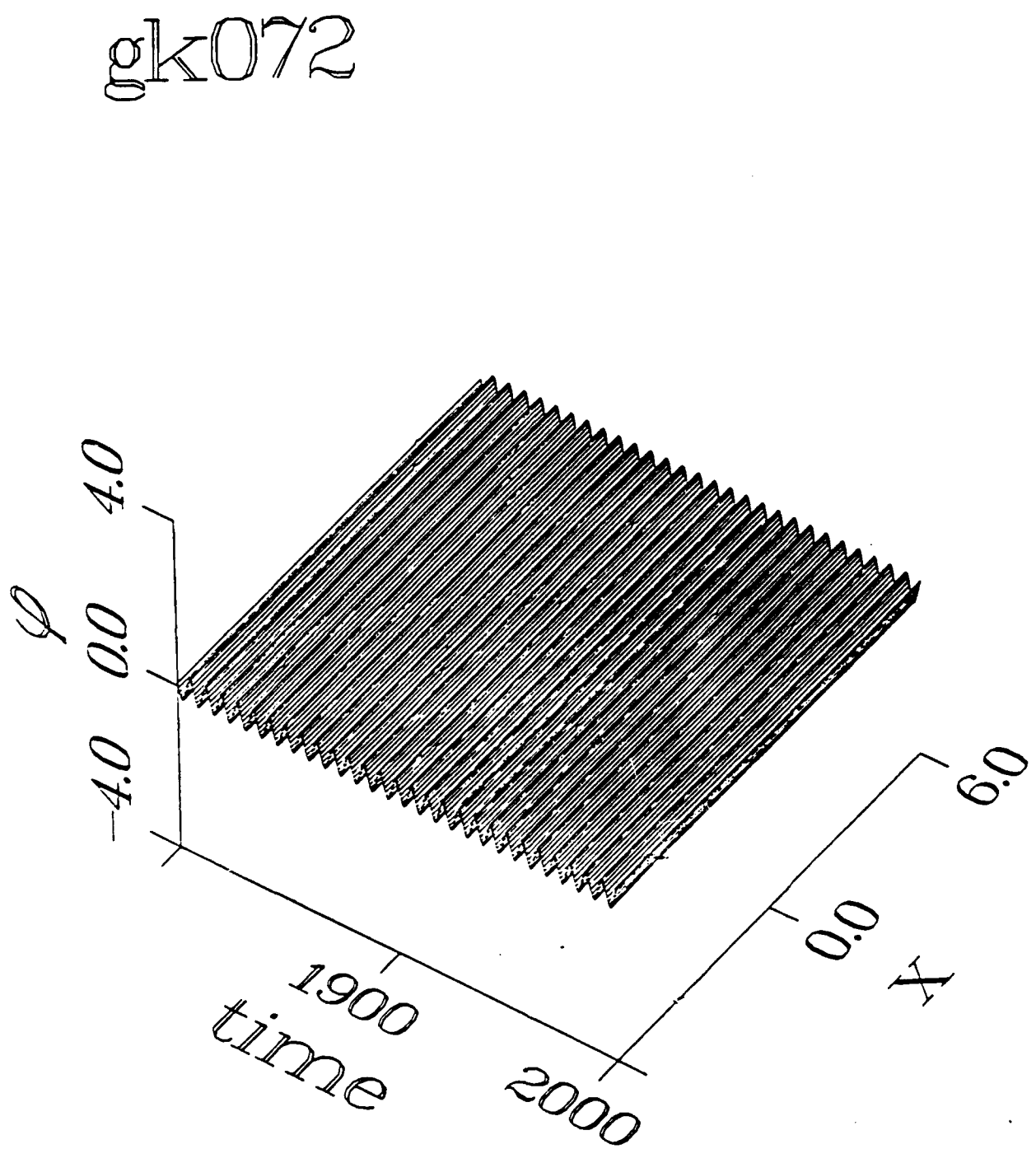

Figure 1 (g)

gk075m

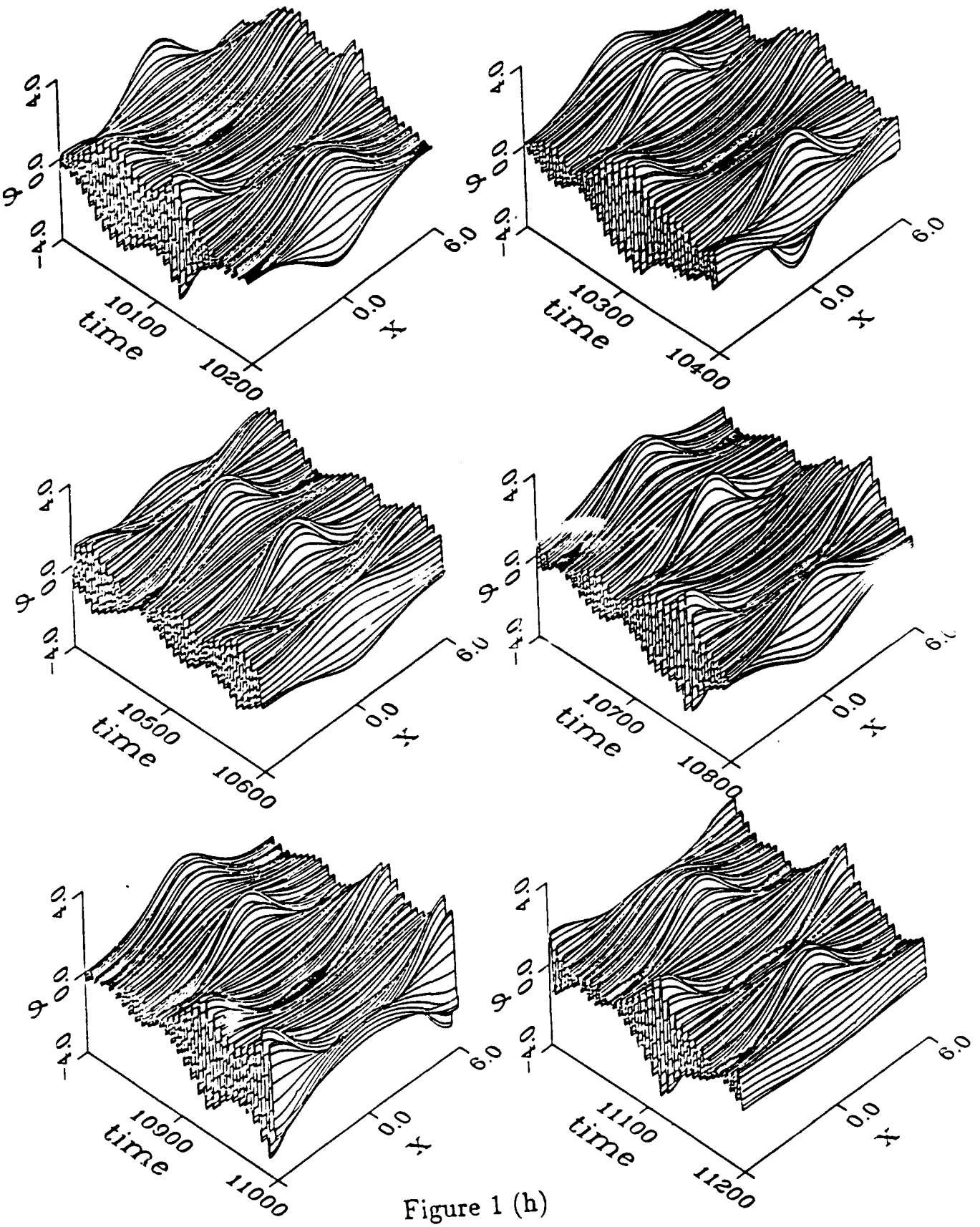

Figure 1 (h)

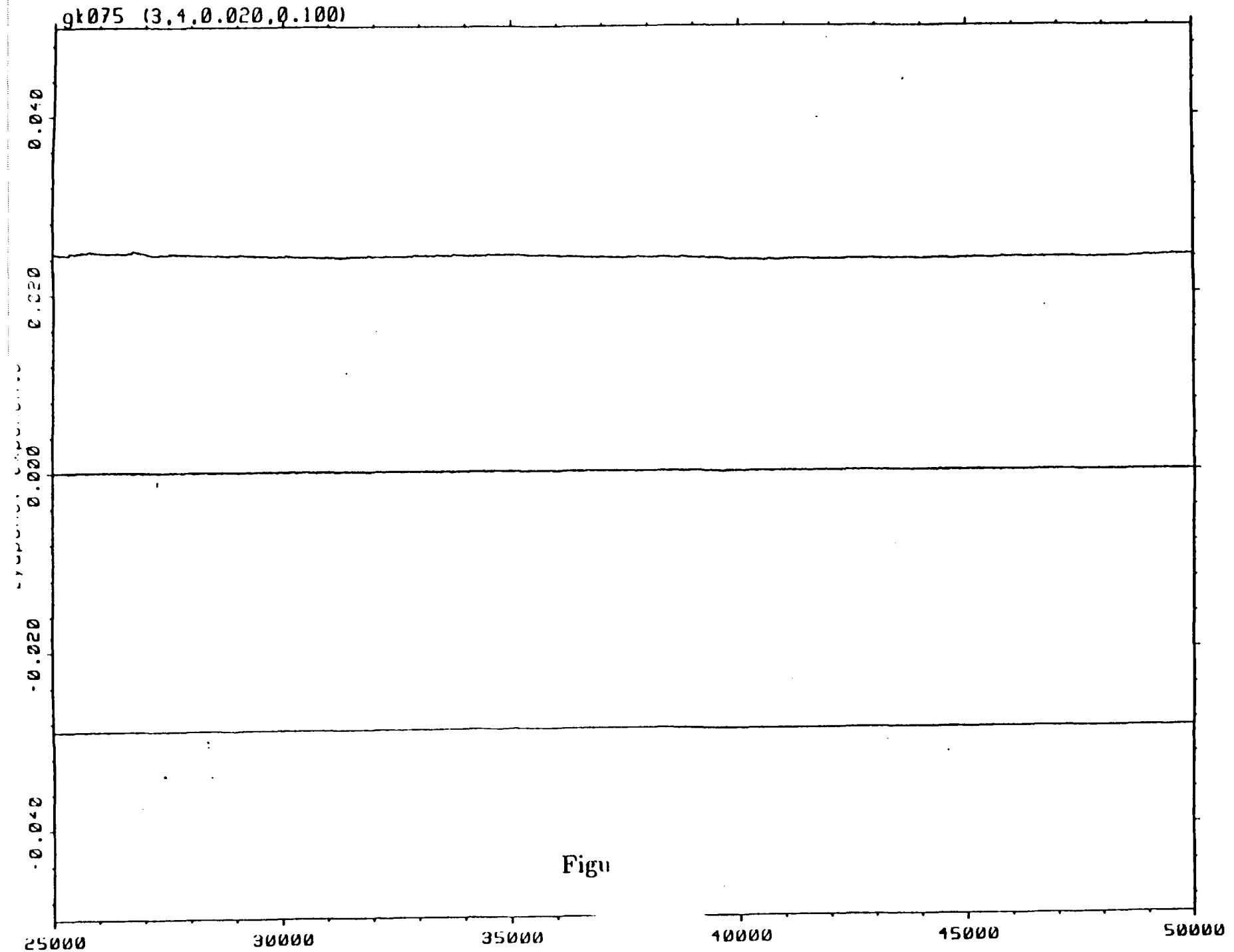
gk075 (3,4,0.020,0.100)
0.040
0.020
0.000
-0.020
-0.040
25000
30000
35000
40000
45000
50000

Figu

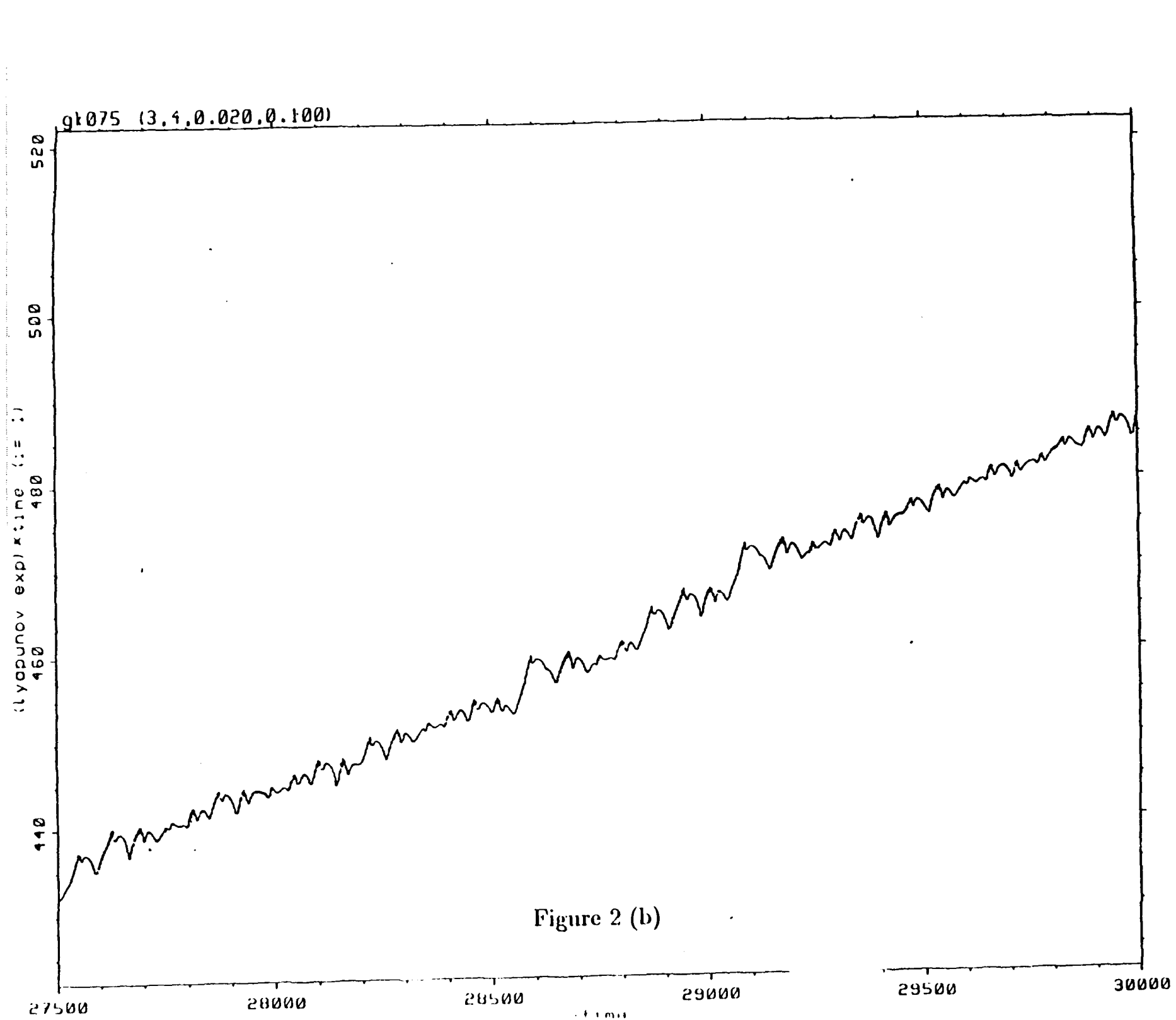
gt075 (3.4,0.020,0.100)
520
500
480
460
440
27500
28000
28500
29000
29500
30000

Figure 2 (b)

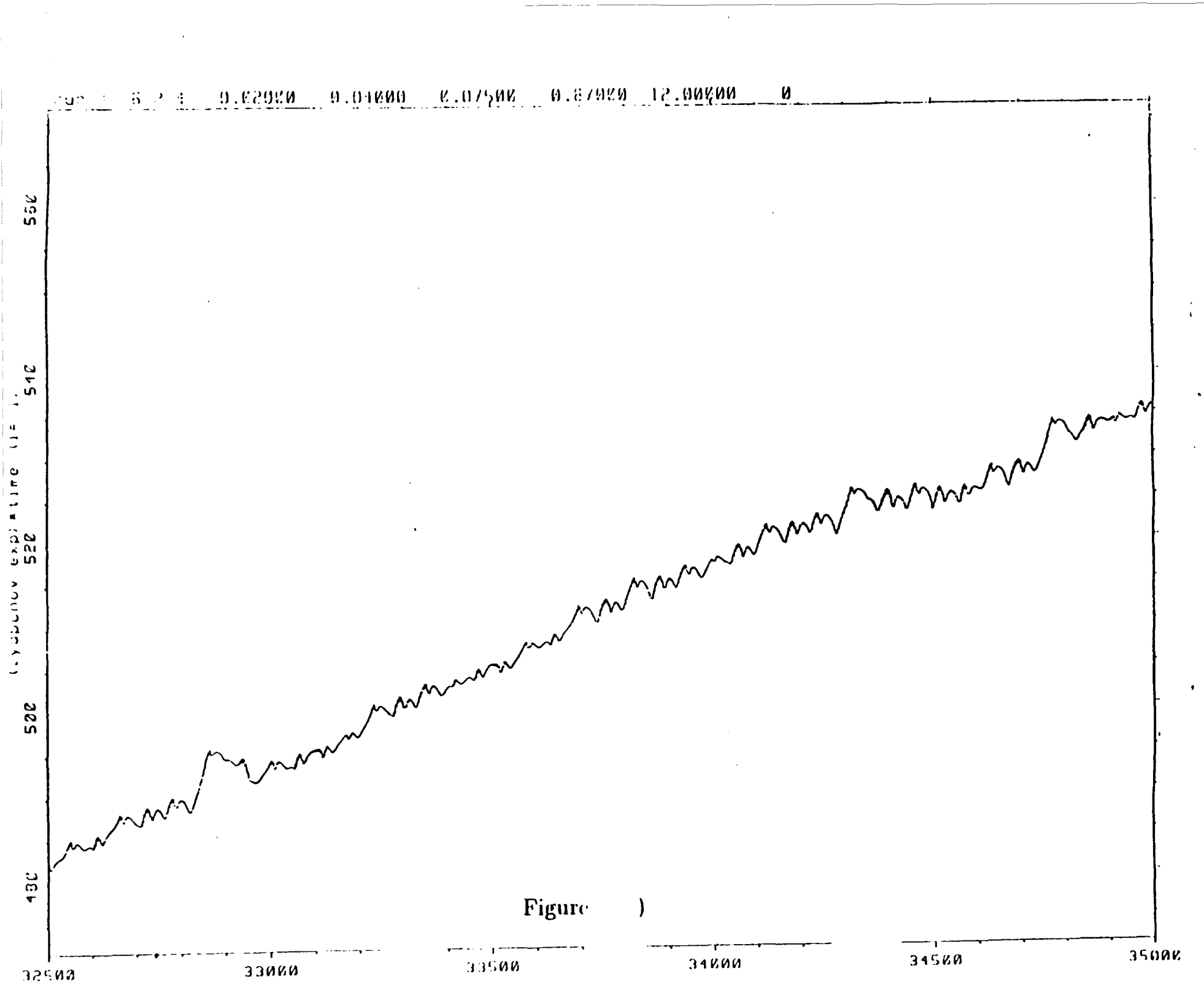

Figure)

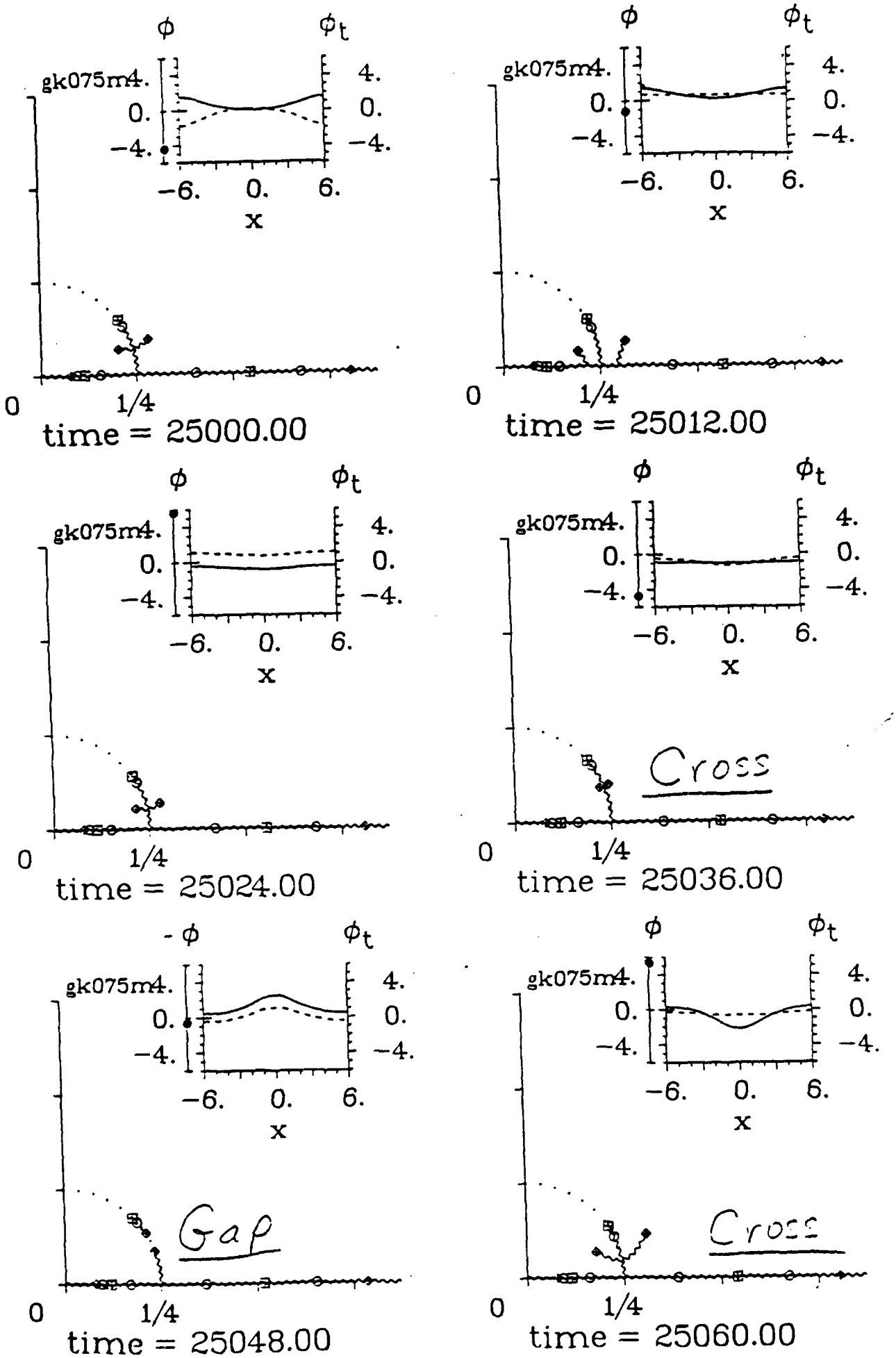
φ
φt
gk075m4.
4.
0.
−4.
−6.
0.
6.
x
0
1/4
time = 25000.00
time = 25012.00
time = 25024.00
time = 25036.00
- φ
Cross
Gap
time = 25048.00
time = 25060.00

Figure 3 (a)

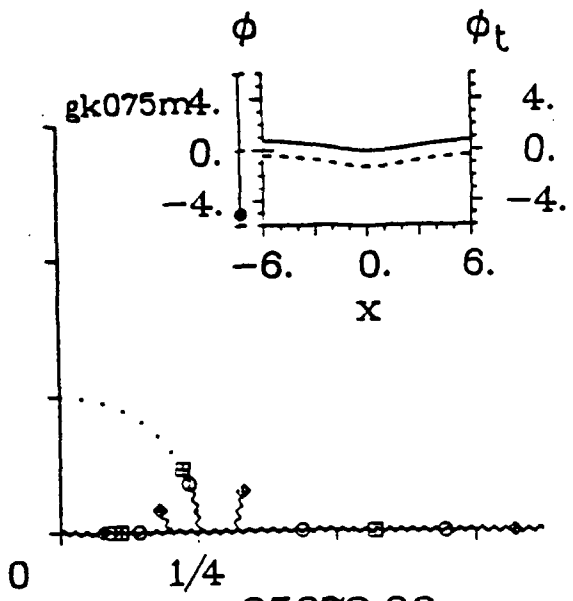

time = 25072.00

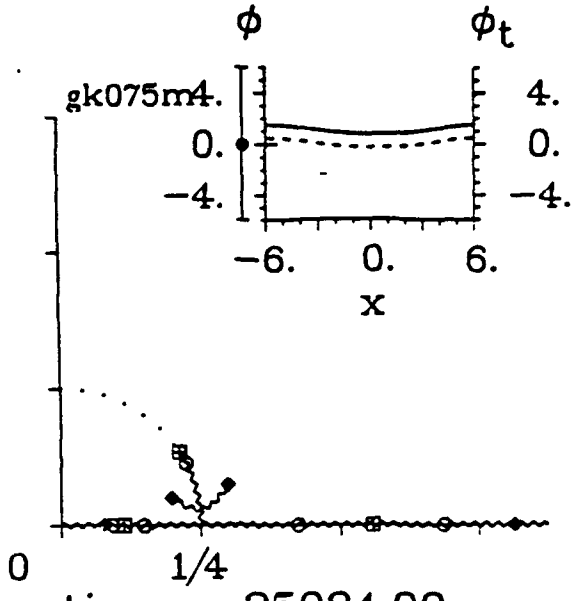

time = 25084.00

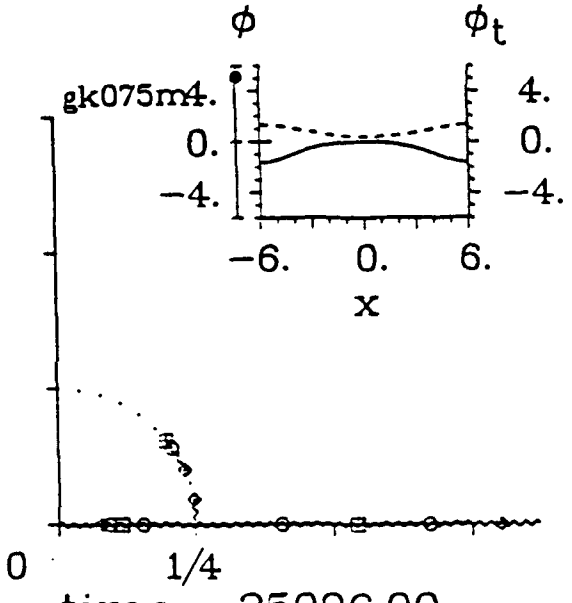

time = 25096.00

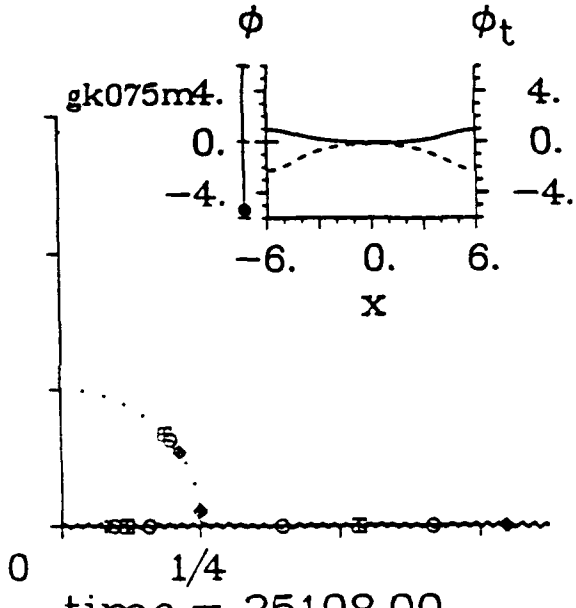

time = 25108.00

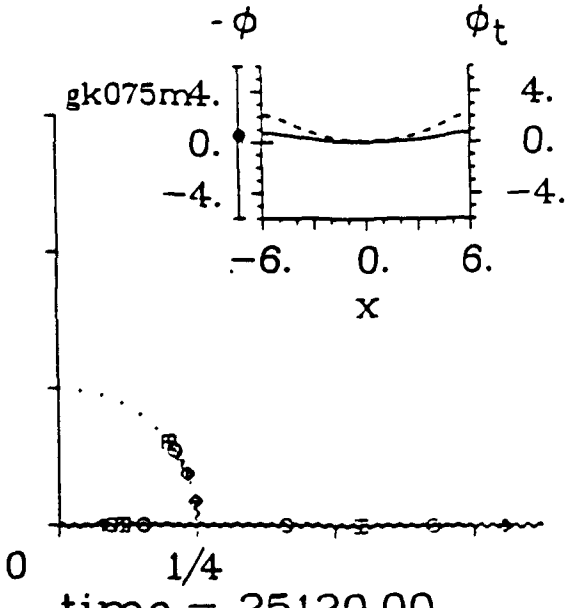

time = 25120.00

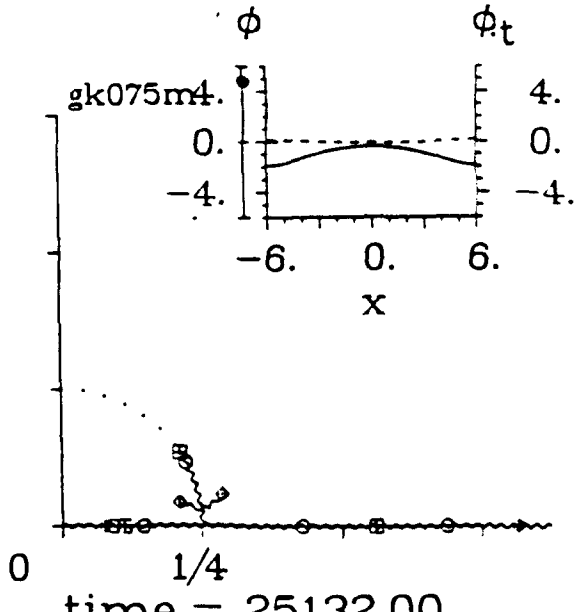

time = 25132.00

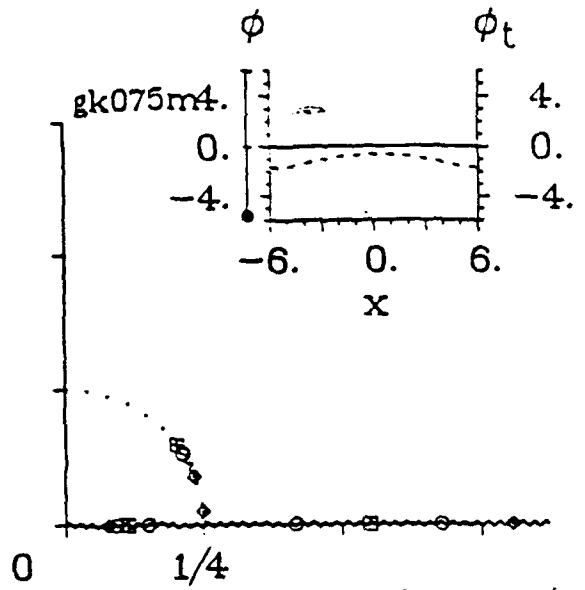

time = 25144.00

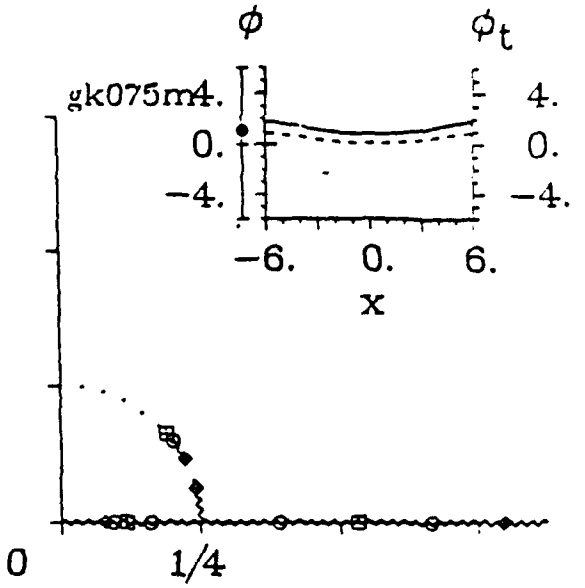

time = 25156.00

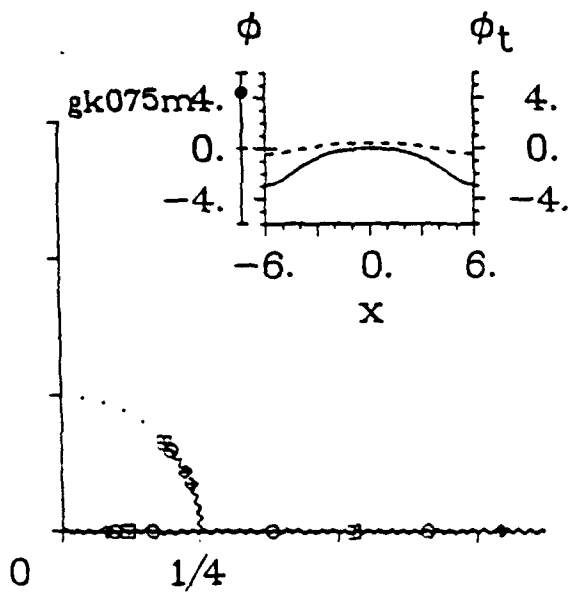

time = 25168.00

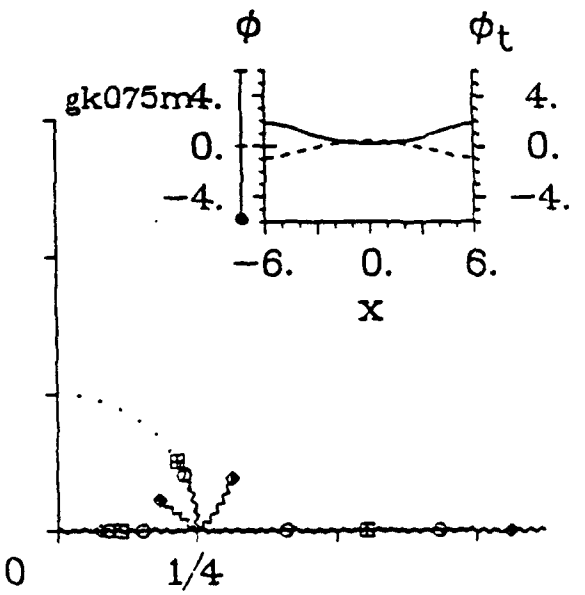

time = 25180.00

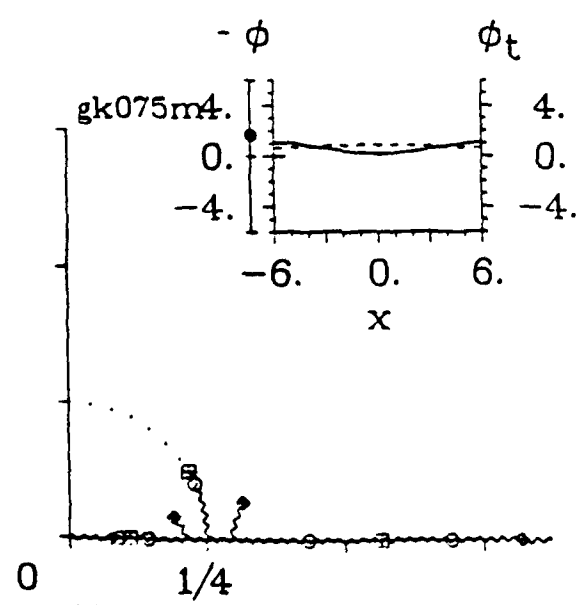

time = 25192.00

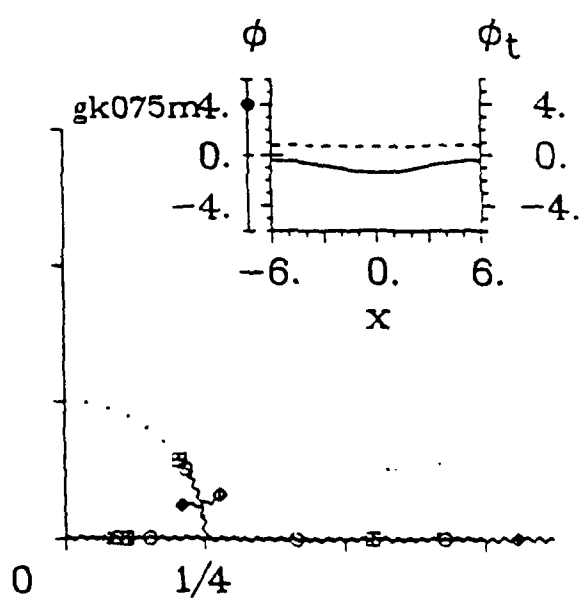

time = 25204.00

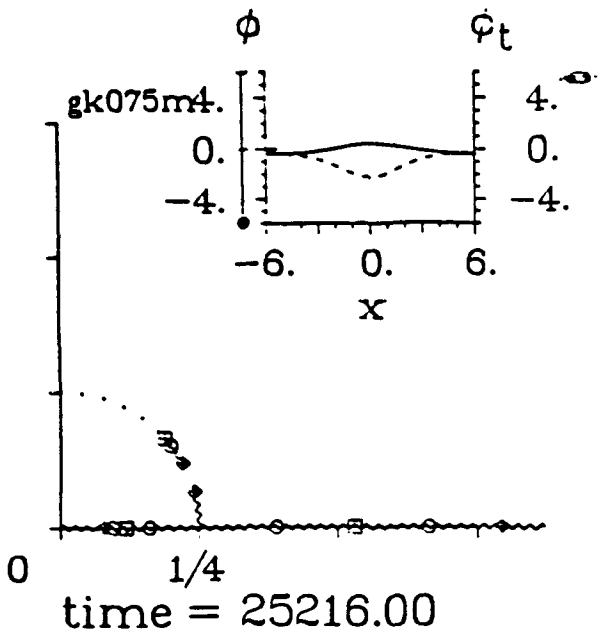

time = 25216.00

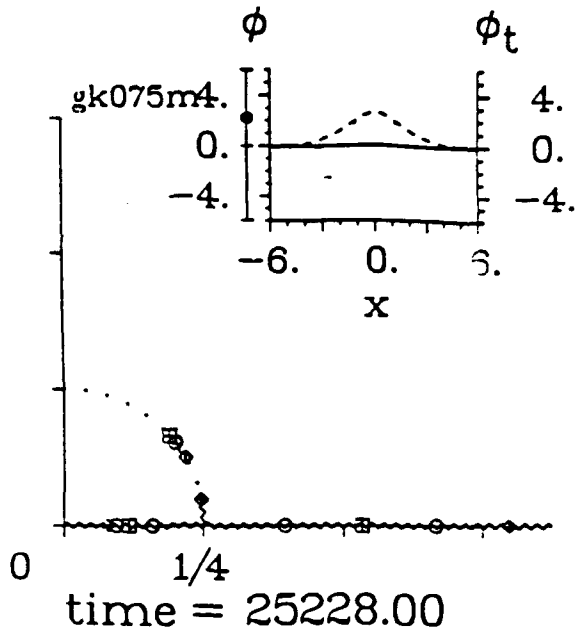

time = 25228.00

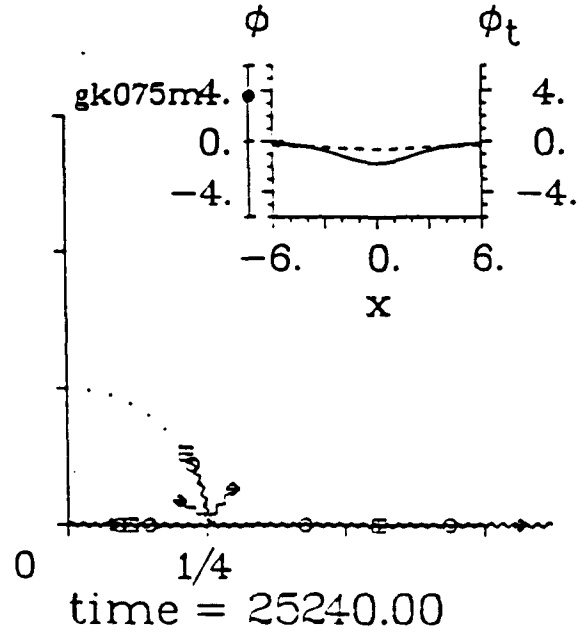

time = 25240.00

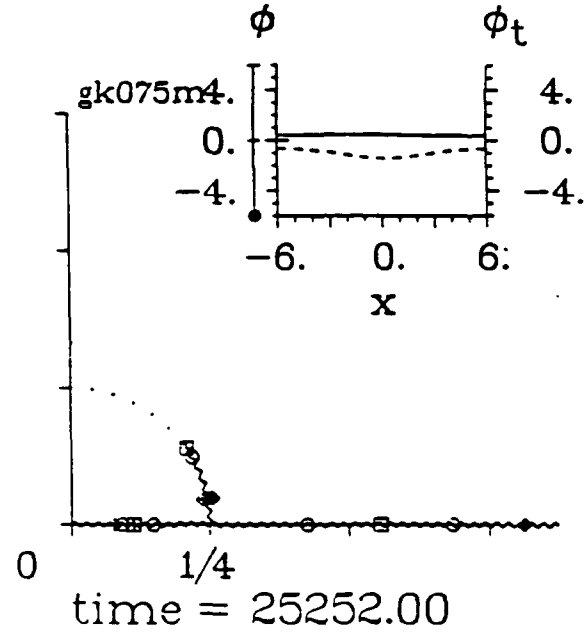

time = 25252.00

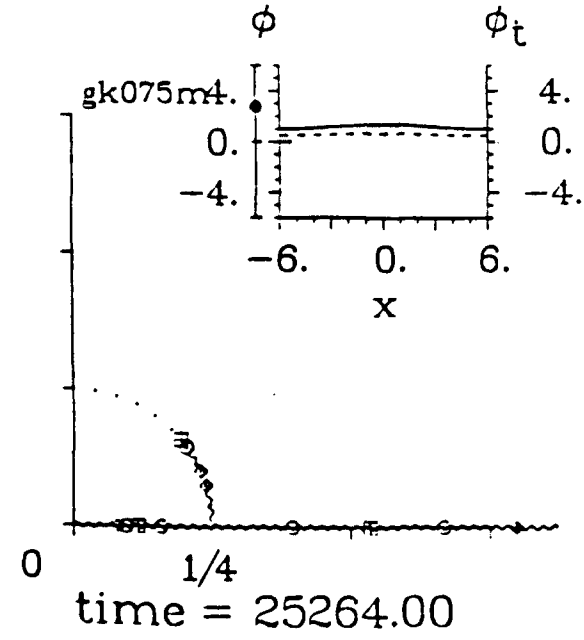

time = 25264.00

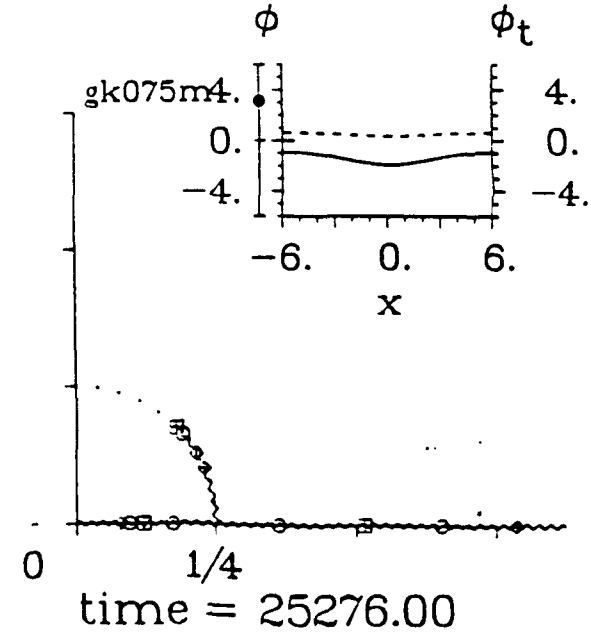

time = 25276.00

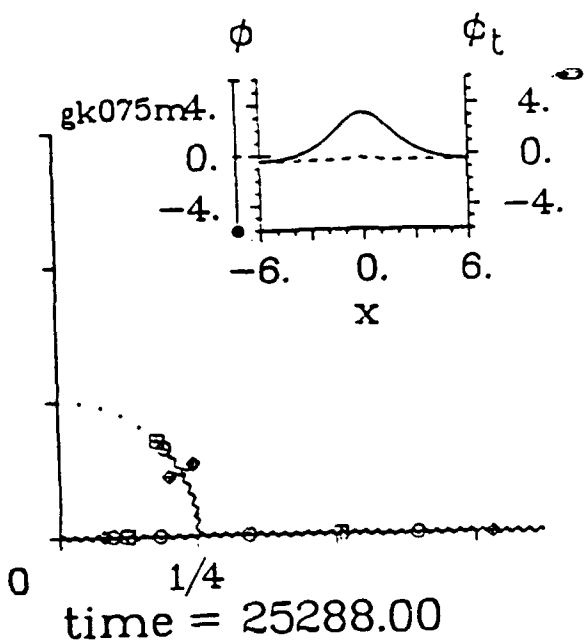
φ
φt
gk075m4.
4.
0.
−4.
0.
−4.
−6.
0.
6.
x
0
1/4
time = 25288.00

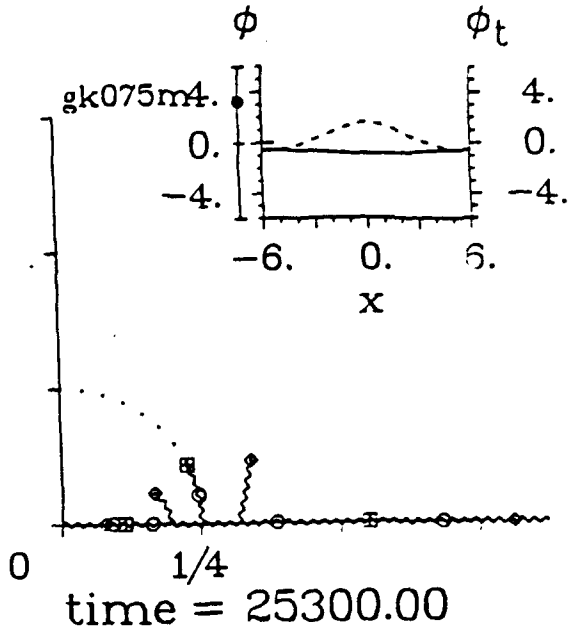
φ
φt
gk075m4.
4.
0.
−4.
0.
−4.
−6.
0.
6.
x
0
1/4
time = 25300.00

gk075m

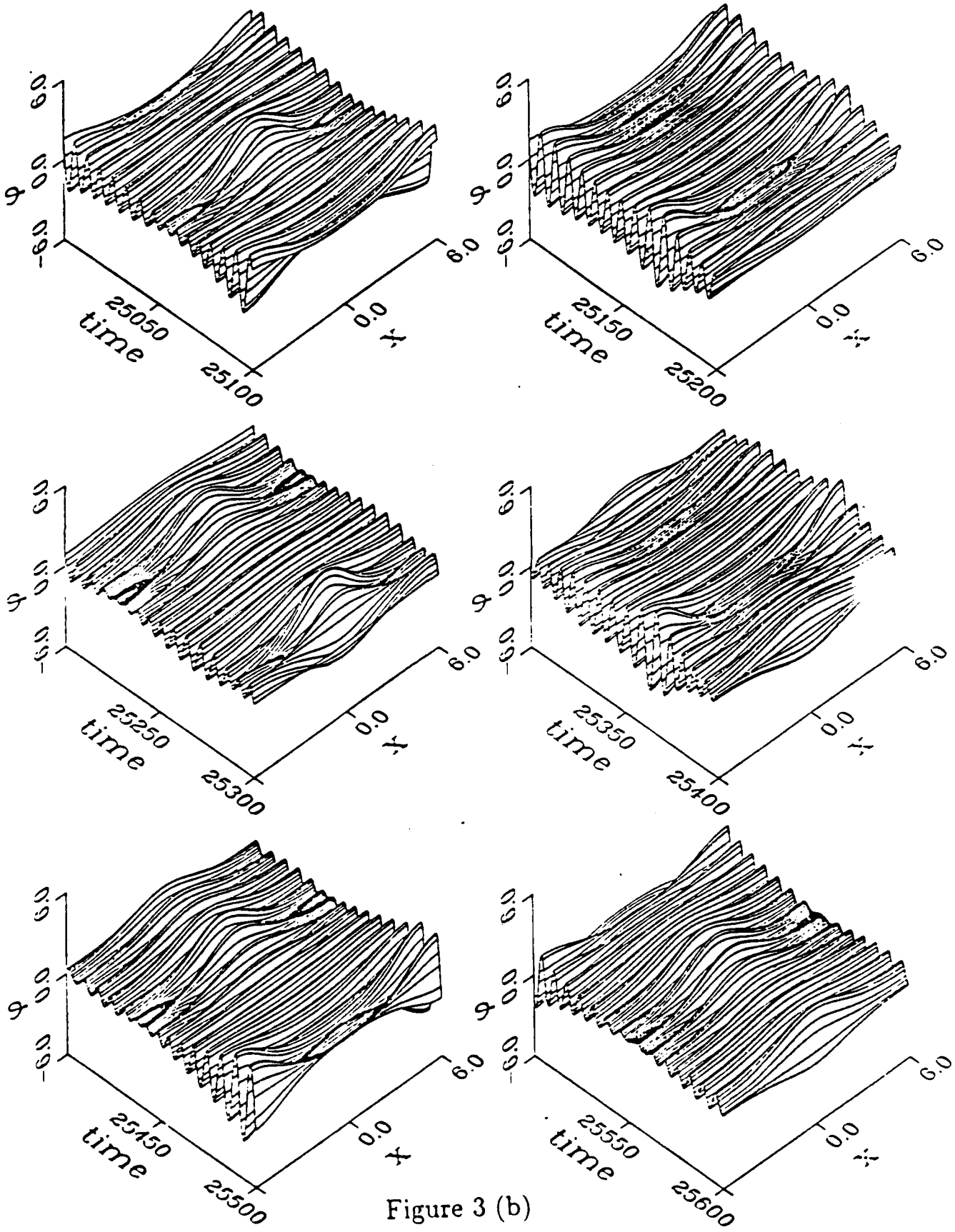

Figure 3 (b)

h12e9.4pi

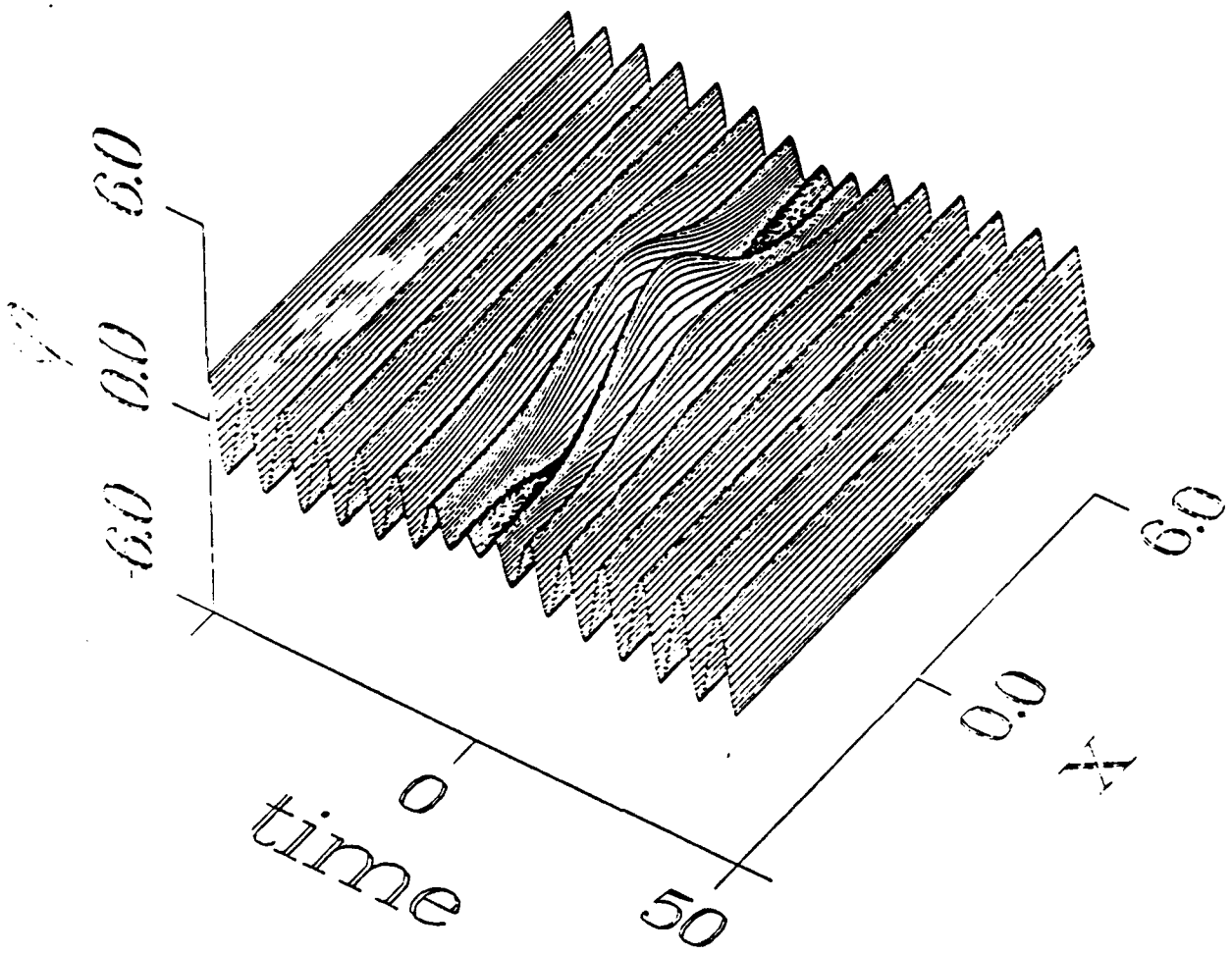

Figure 4 (a)

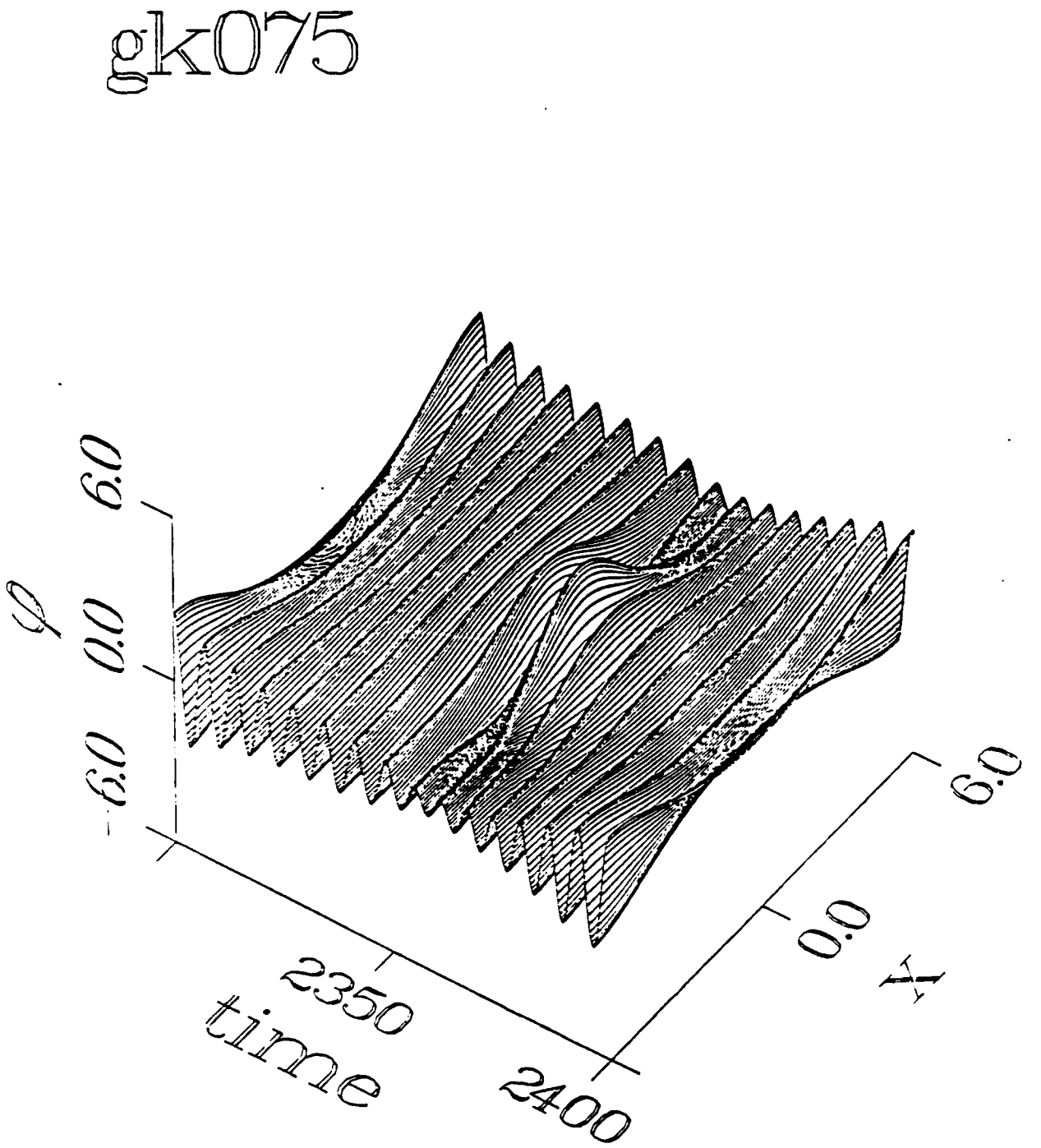

Figure 4 (b)

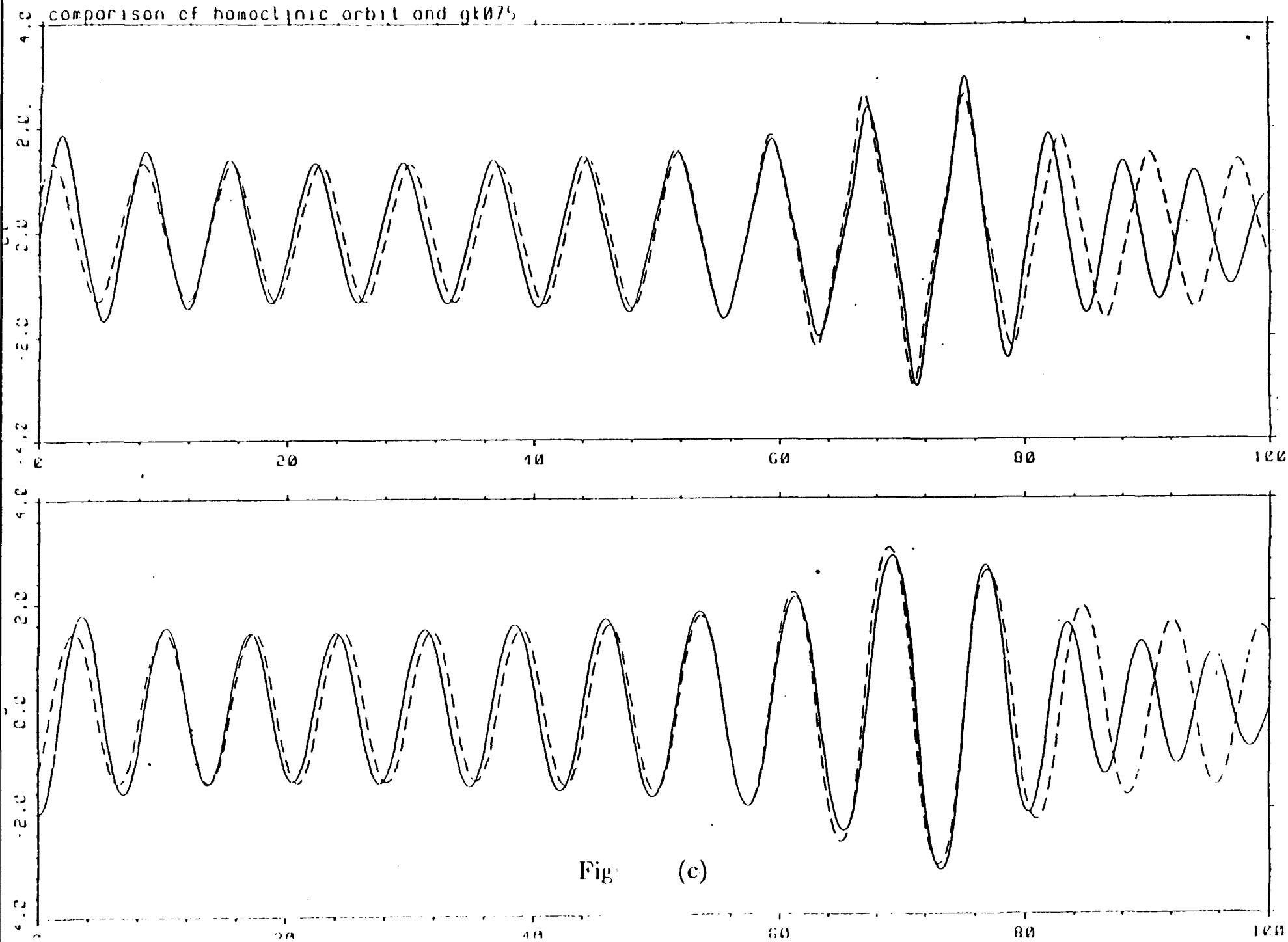
comparison of homoclinic orbit and gk075
4.0
2.0
0.0
-2.0
-4.2
0
20
40
60
80
100

Fig (c)

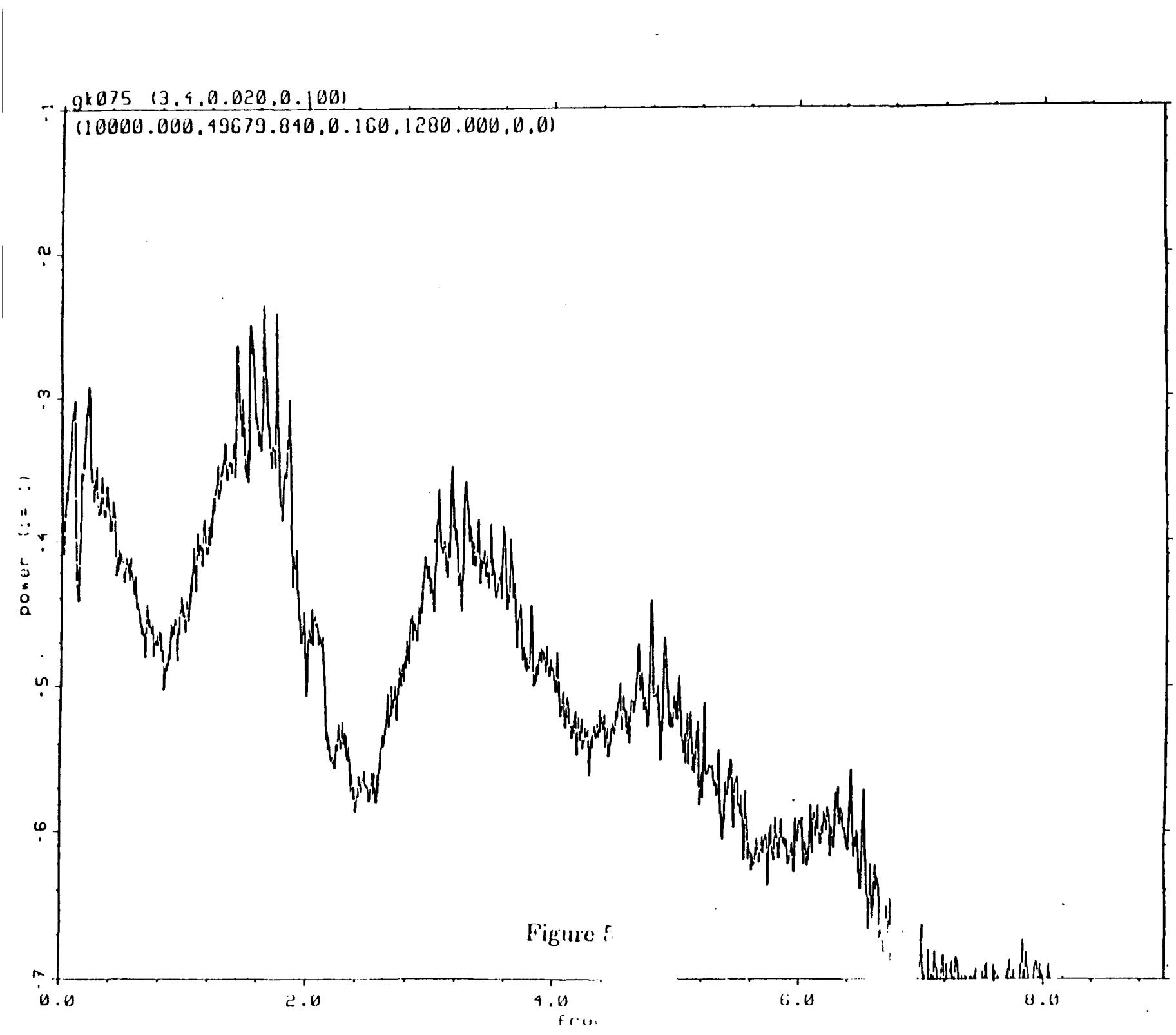
gk075 (3,4,0.020,0.100)
(10000.000,49679.840,0.160,1280.000,0,0)
power
0.0
2.0
4.0
6.0
8.0

Figure 5

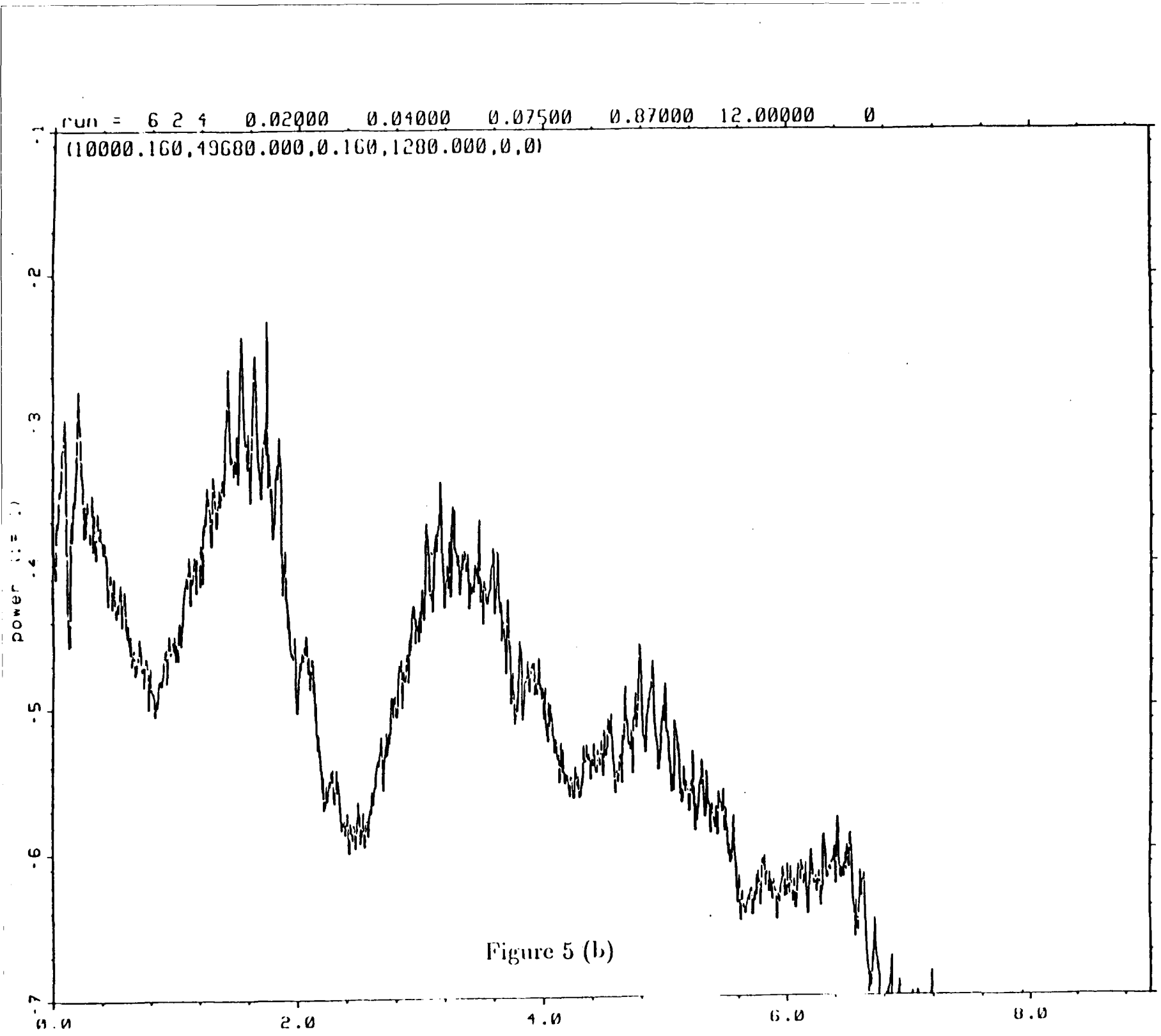
run = 6 2 4 0.02000 0.04000 0.07500 0.87000 12.00000 0
(10000.160,49680.000,0.160,1280.000,0,0)
power
.1
.2
.3
.4
.5
.6
.7
2.0
4.0
6.0
8.0

Figure 5 (b)

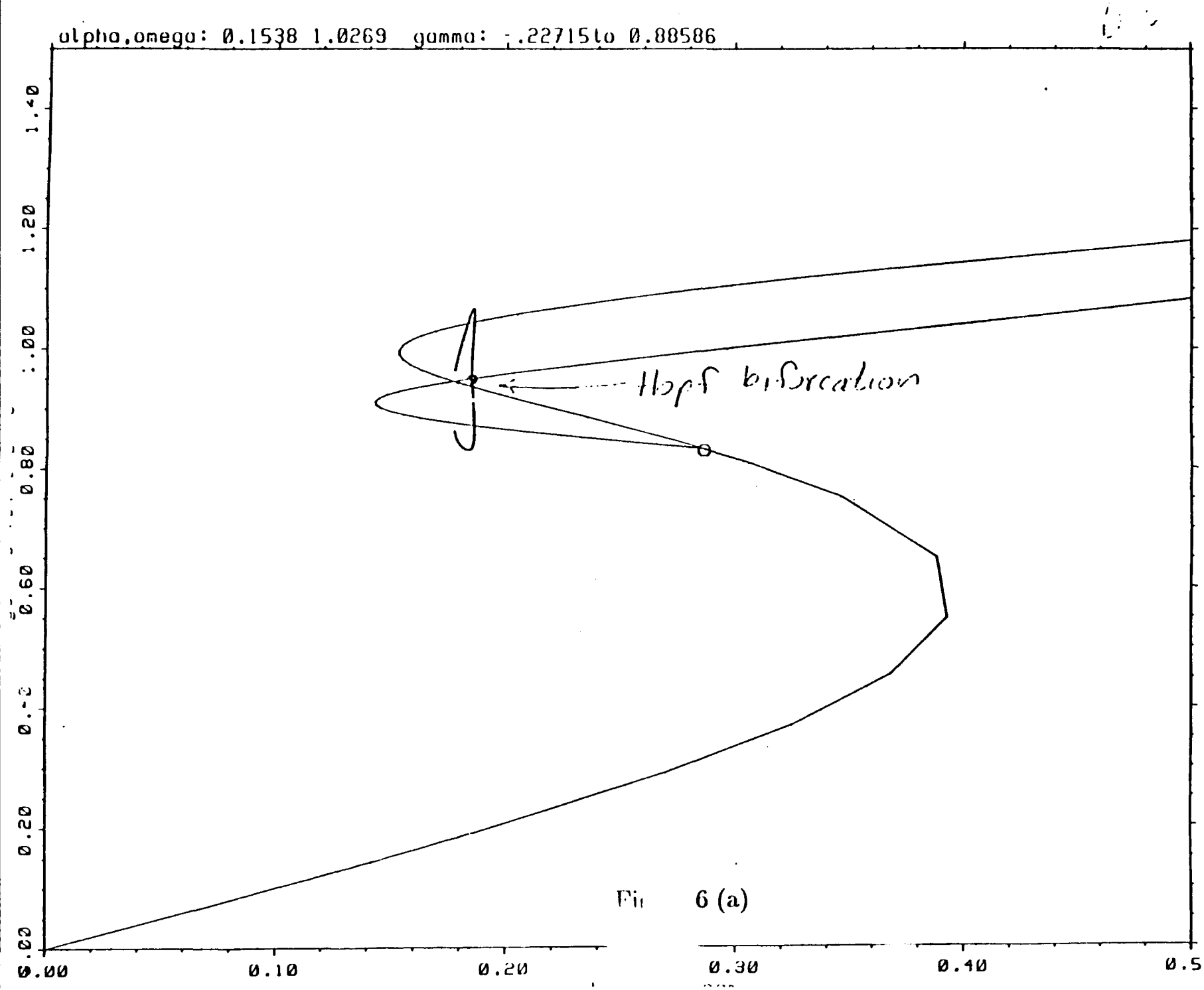
alpha,omega: 0.1538 1.0269 gamma: -.22715to 0.88586
1.40
1.20
1.00
0.80
0.60
0.20
0.00
0.00
0.10
0.20
0.30
0.40
0.50
Hopf bifurcation

Fi 6 (a)

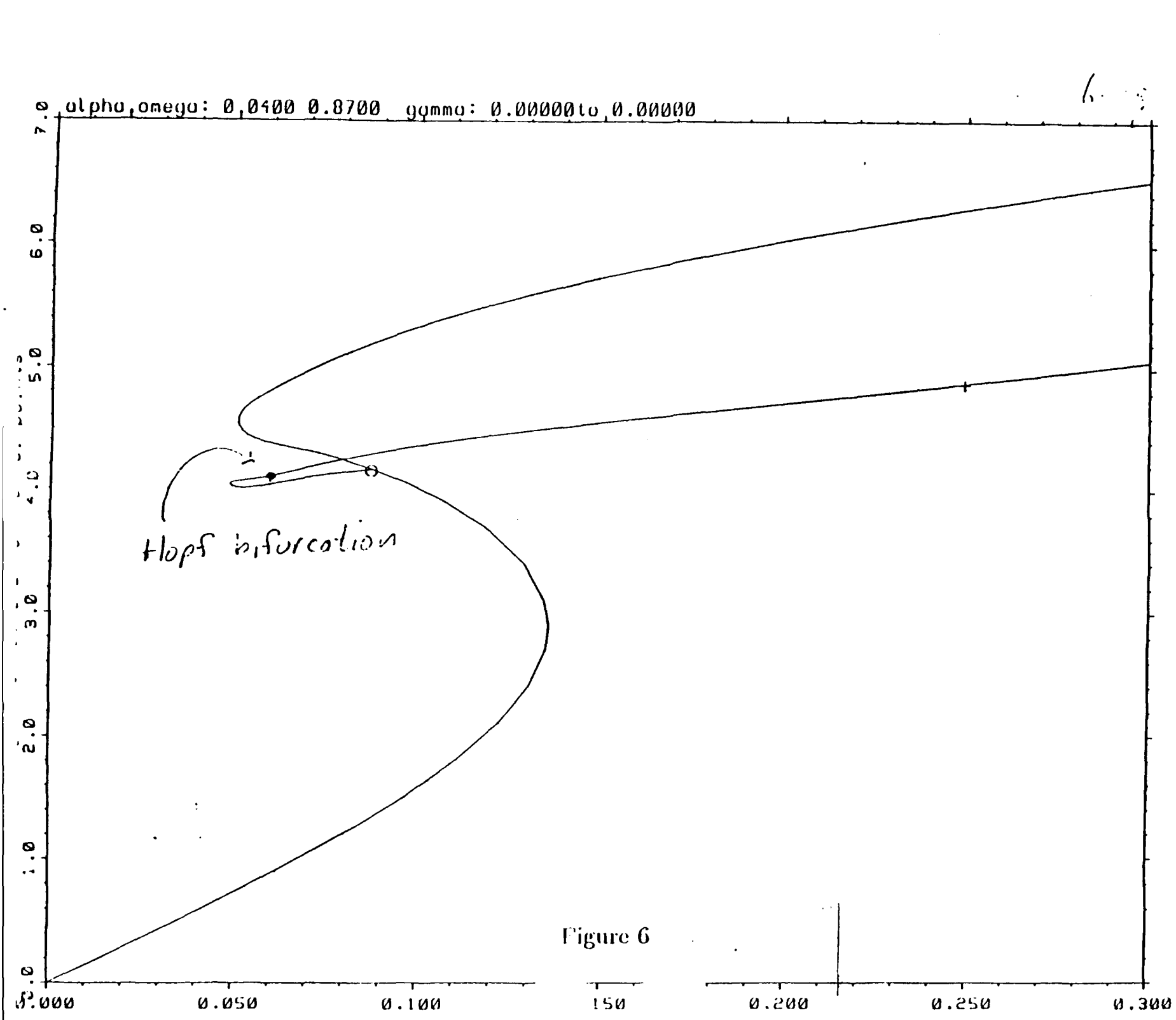
alpha,omega: 0.0400 0.8700 gamma: 0.00000 to 0.00000
7.0
6.0
5.0
4.0
3.0
2.0
1.0
0.000
0.050
0.100
150
0.200
0.250
0.300
Hopf bifurcation

Figure 6

m0043

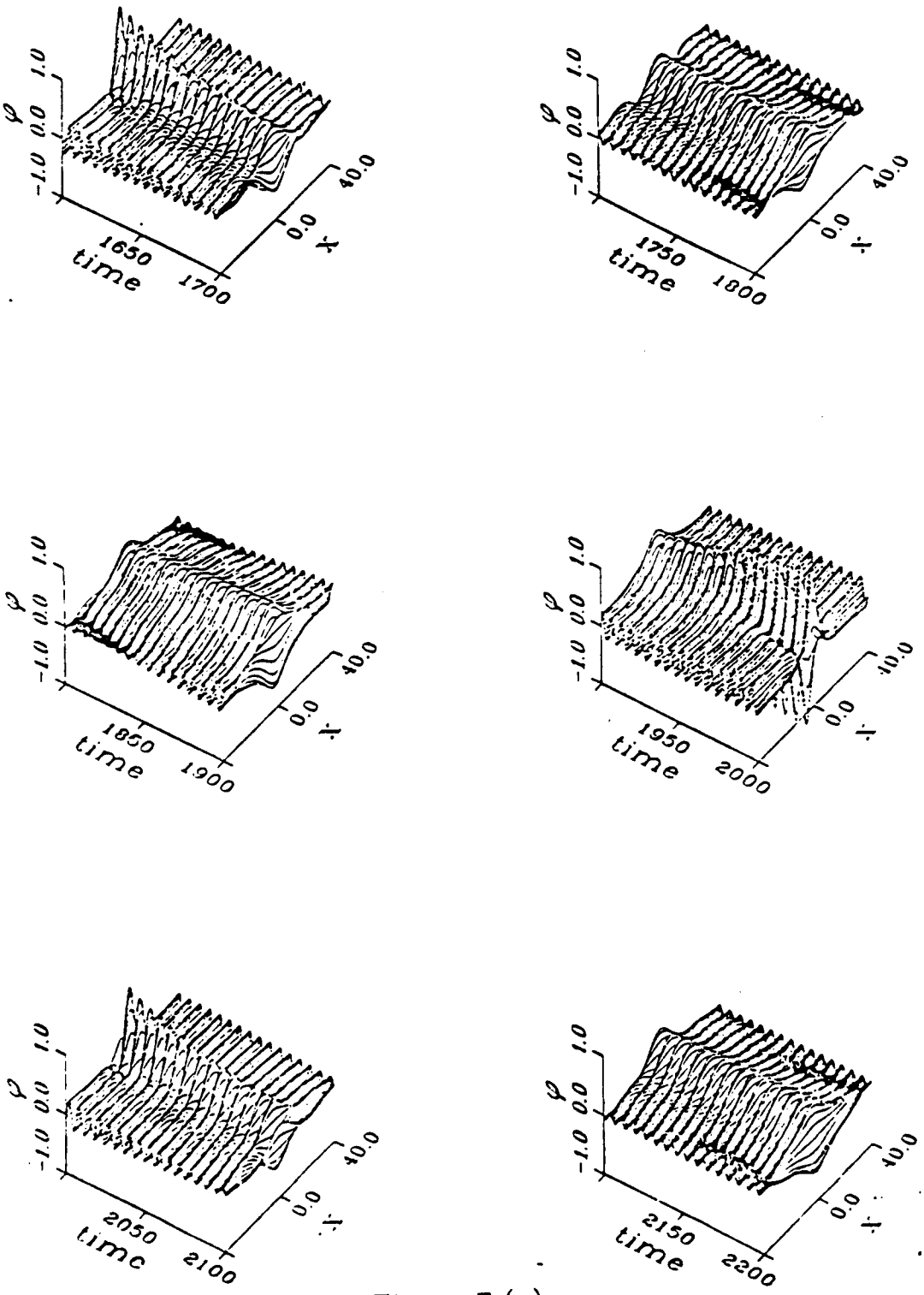

Figure 7 (a)

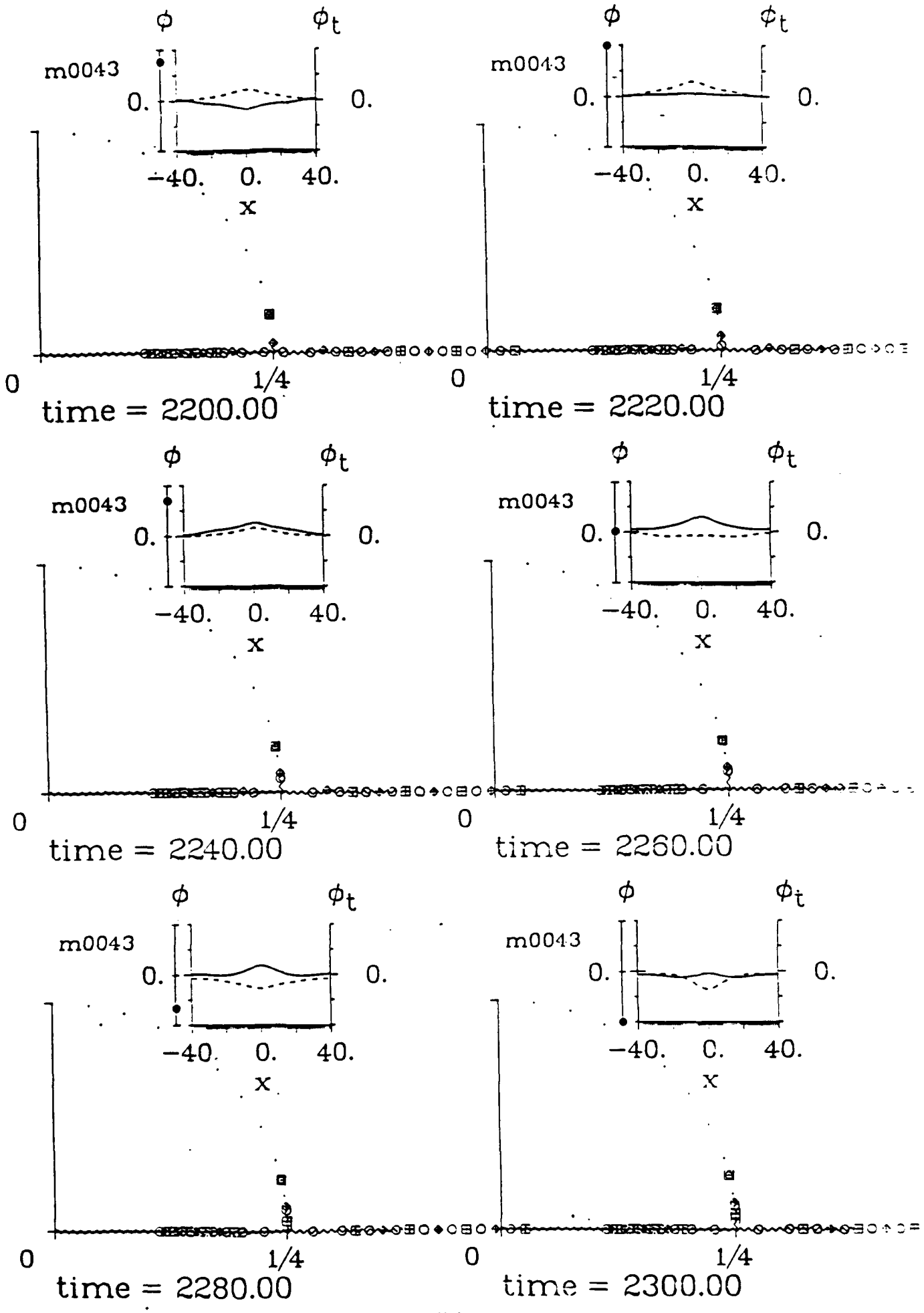
φ
φt
m0043
0.
0.
−40.
0.
40.
x
0
1/4
time = 2200.00
time = 2220.00
time = 2240.00
time = 2260.00
time = 2280.00
time = 2300.00

Figure 7 (b)

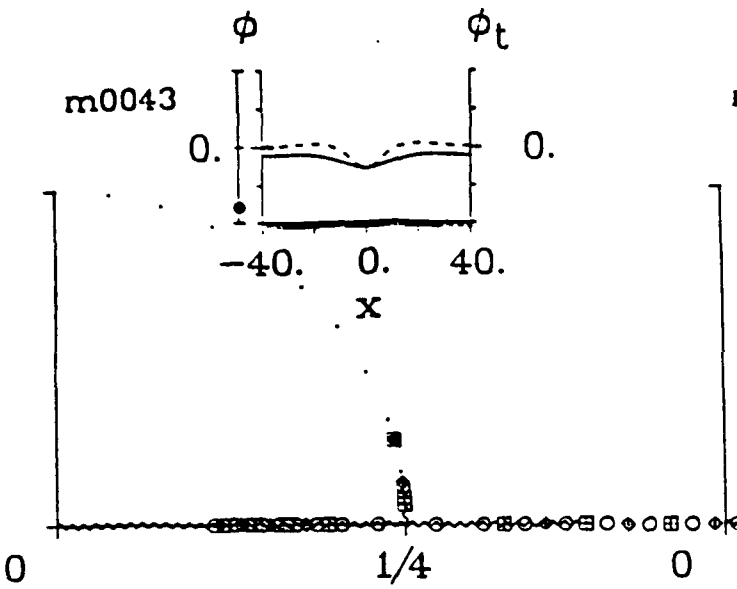

time = 2320.00

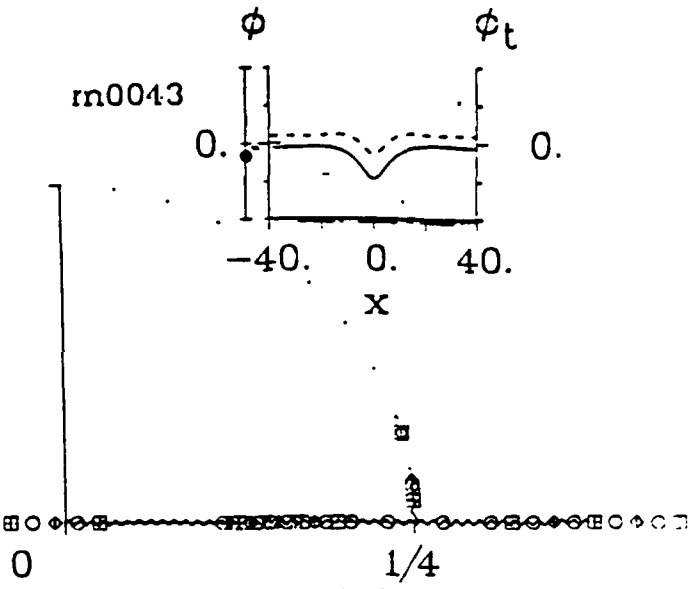

time = 2340.00

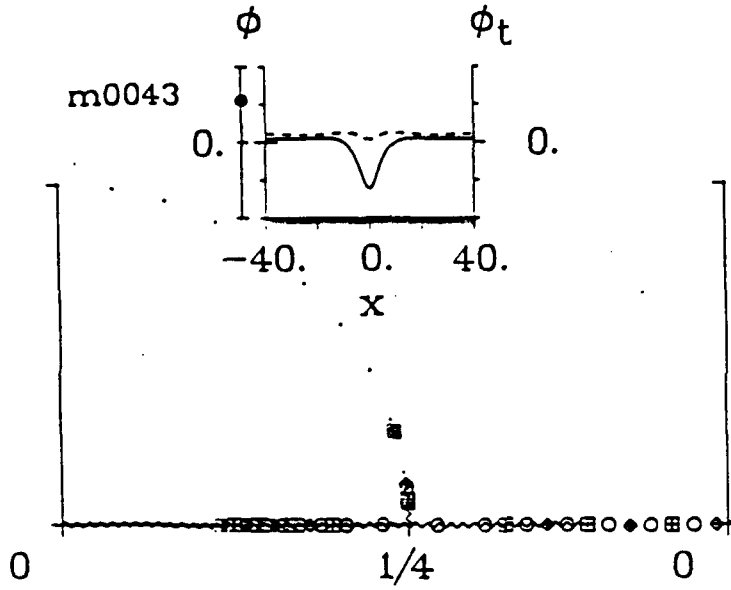

time = 2360.00

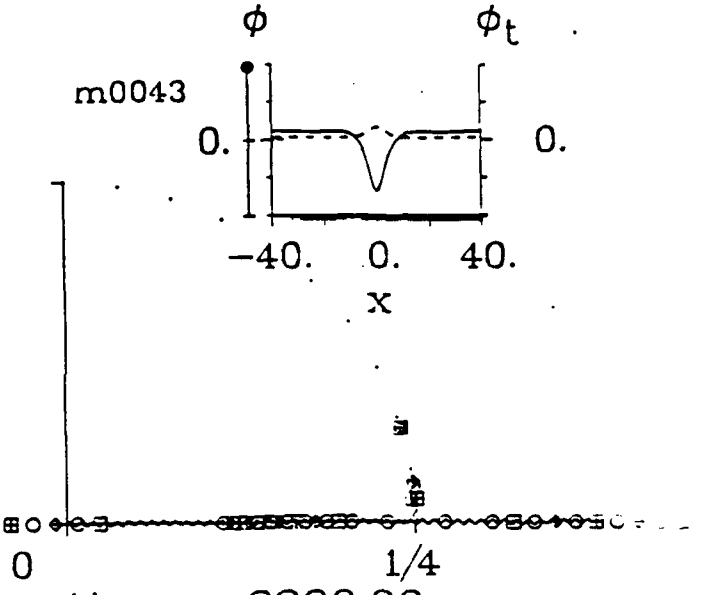

time = 2380.00

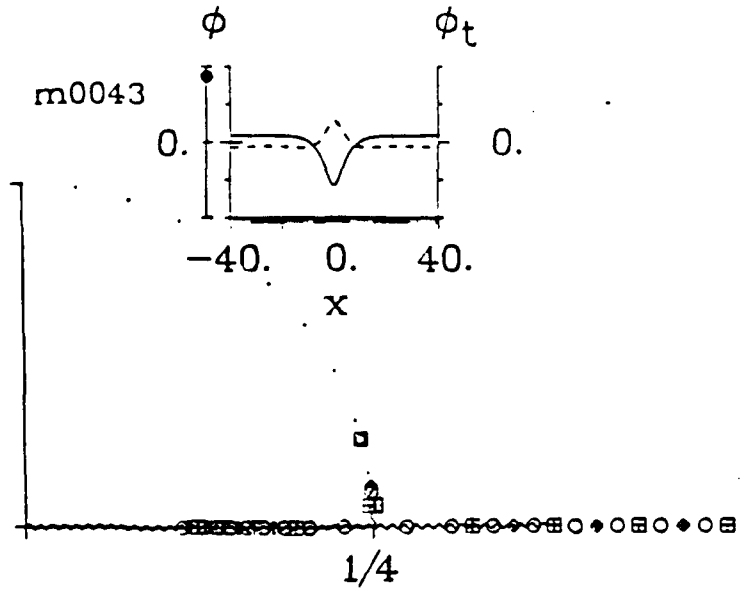

time = 2400.00

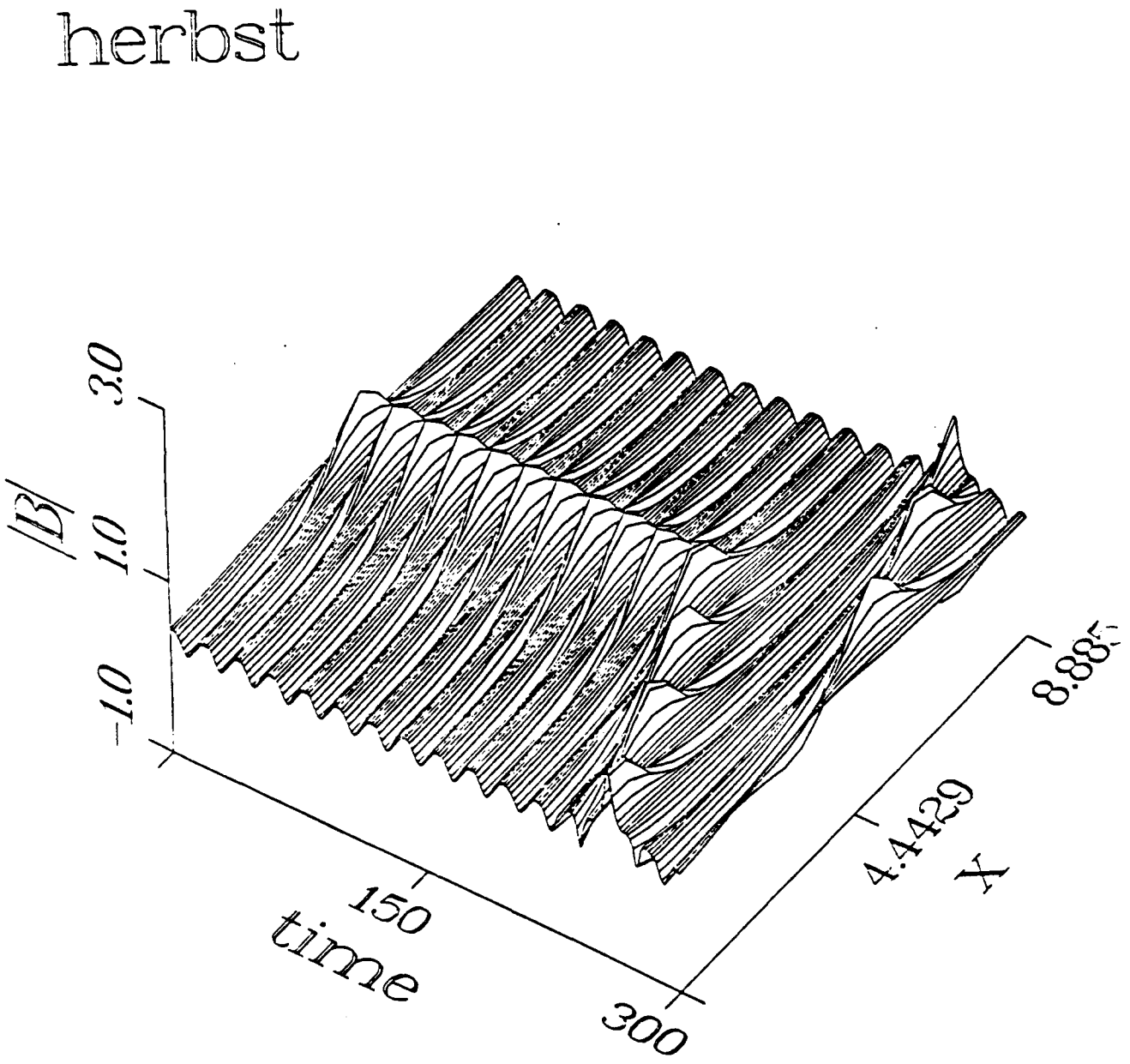

Figure 8 (a)

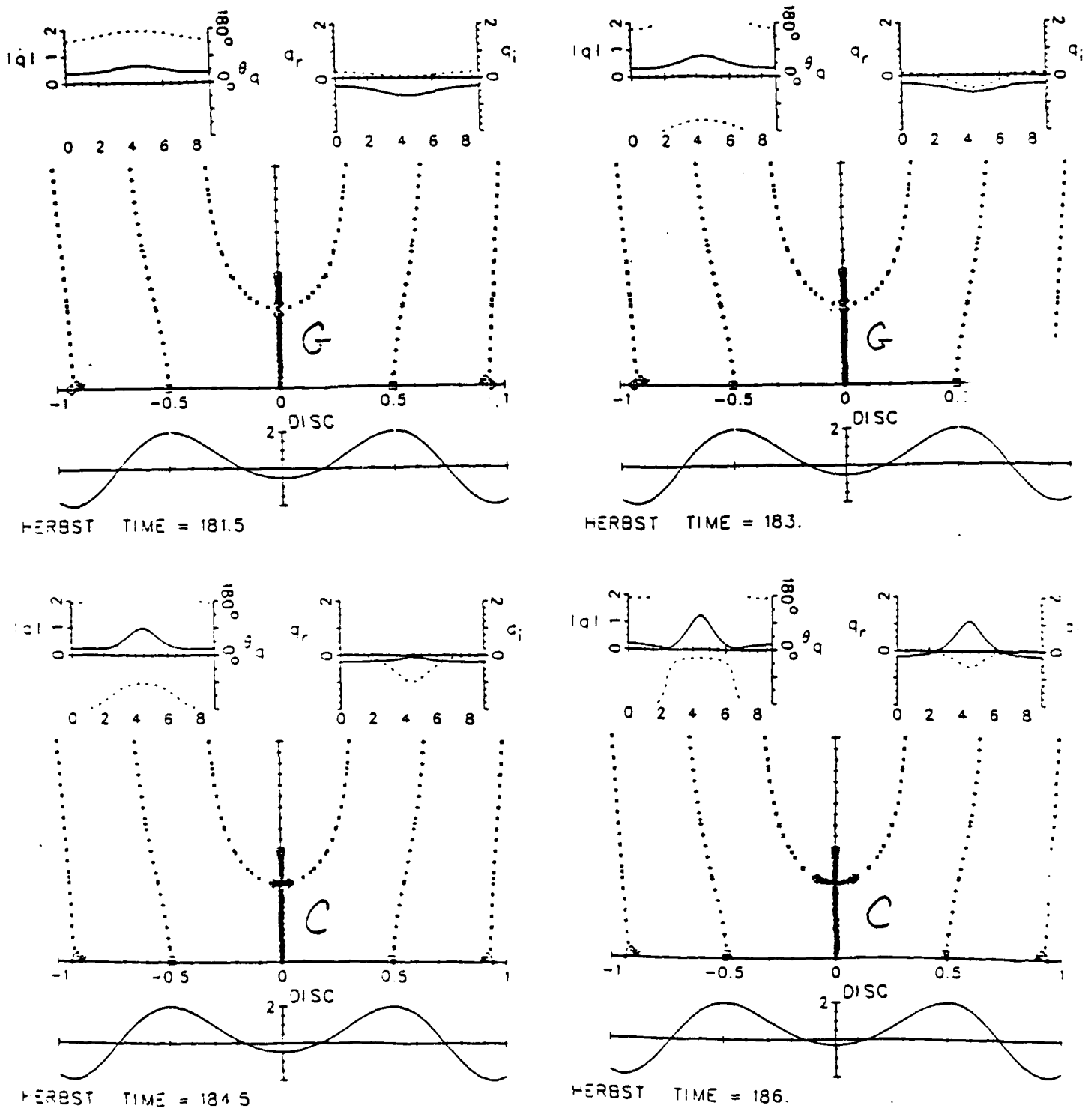
|q|
θq
qr
qi
DISC
G
C
HERBST TIME = 181.5
HERBST TIME = 183.
HERBST TIME = 184.5
HERBST TIME = 186.

Figure 8 (b)

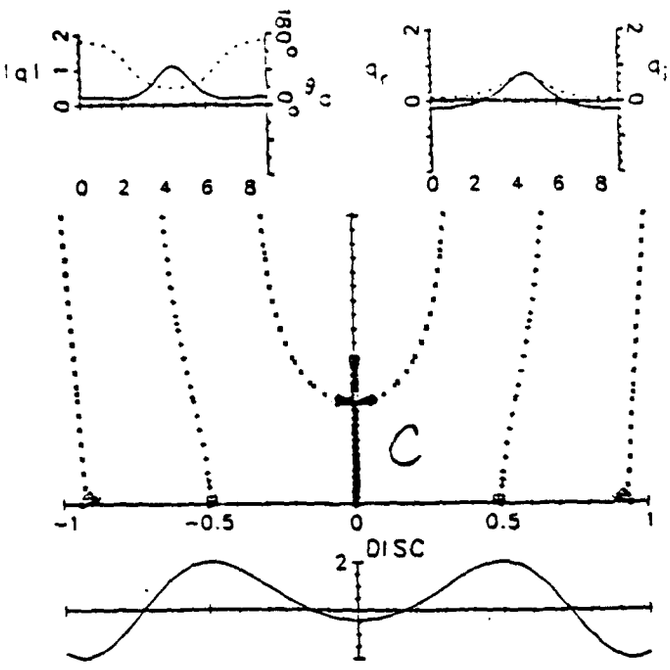

HERBST TIME = 187.5

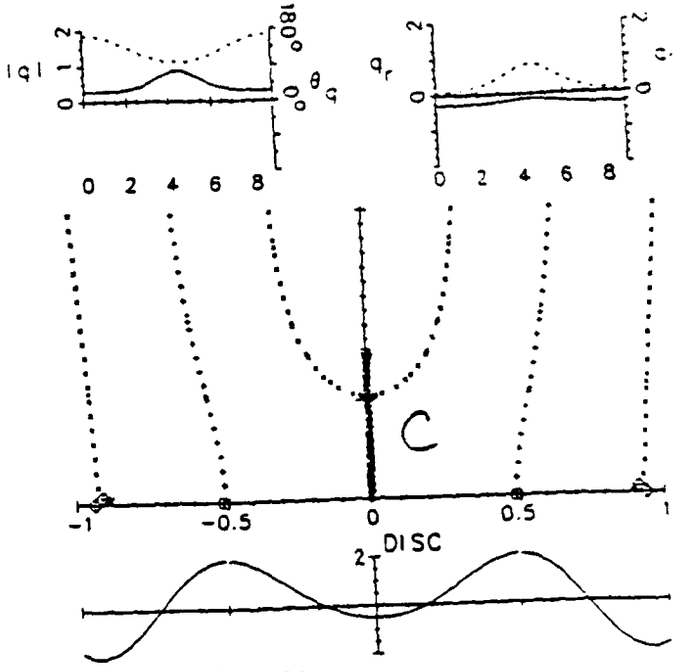

HERBST TIME = 189.

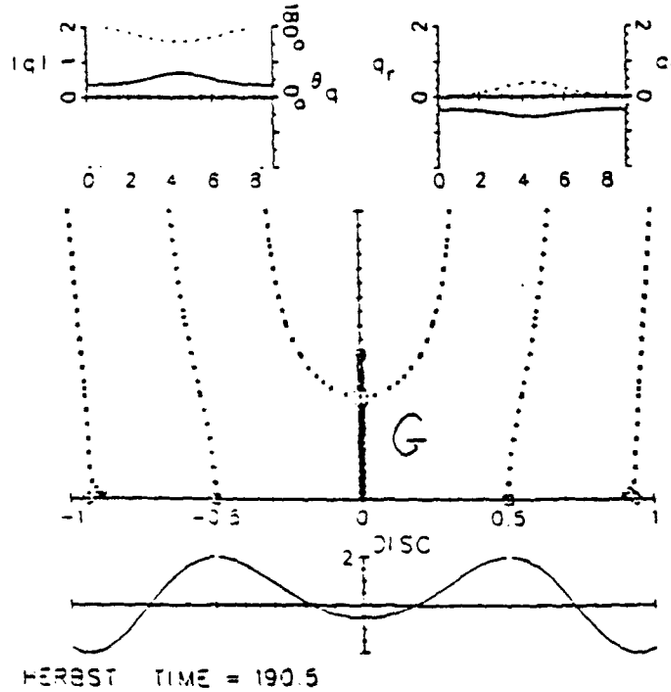

HERBST TIME = 190.5

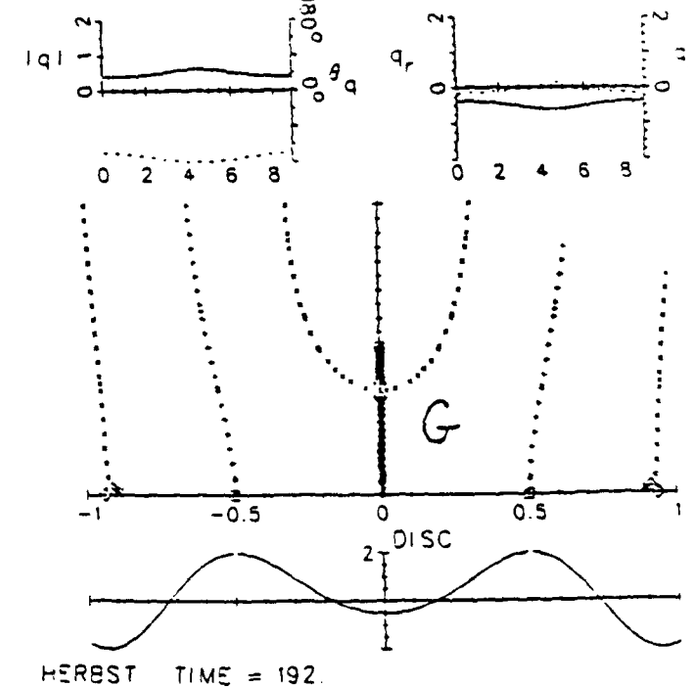

HERBST TIME = 192.

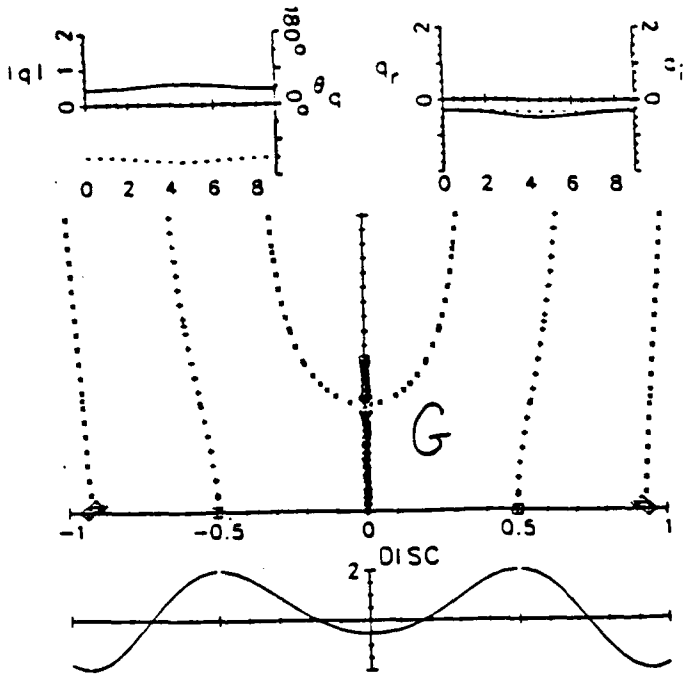

HERBST TIME = 193.5

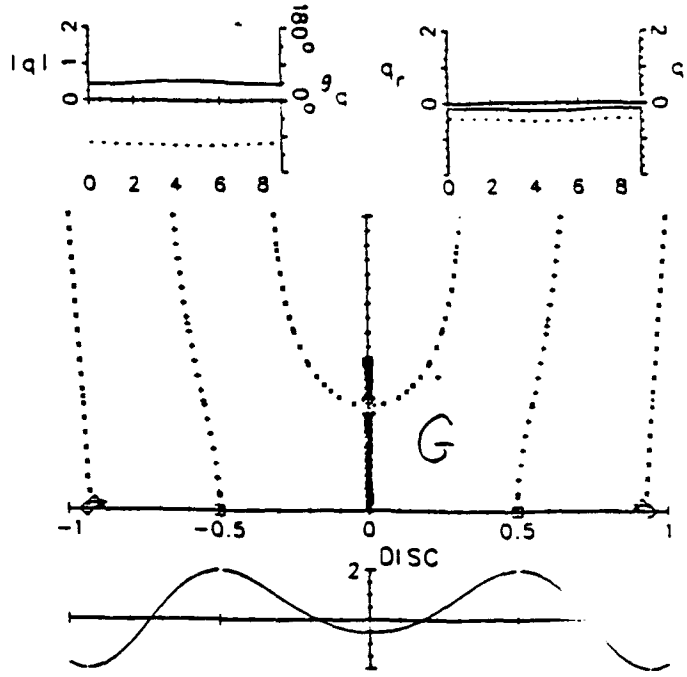

HERBST TIME = 195.

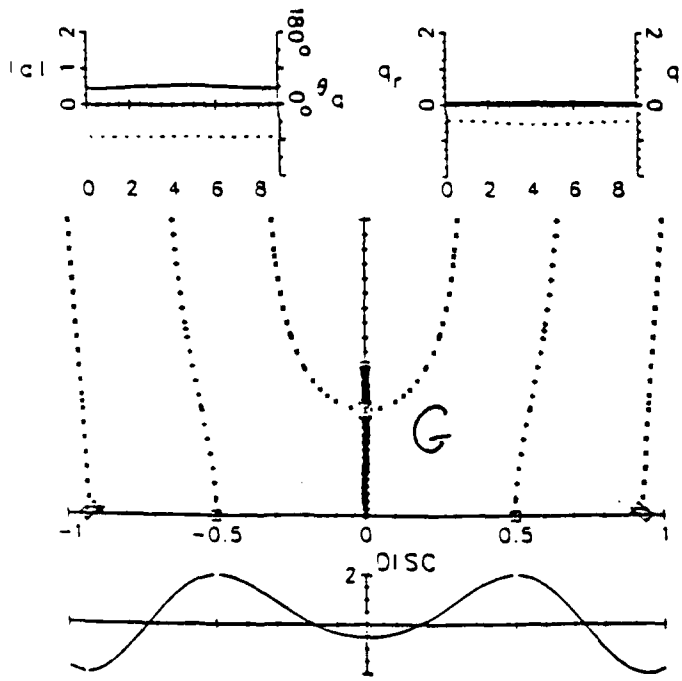

HERBST TIME = 196.5

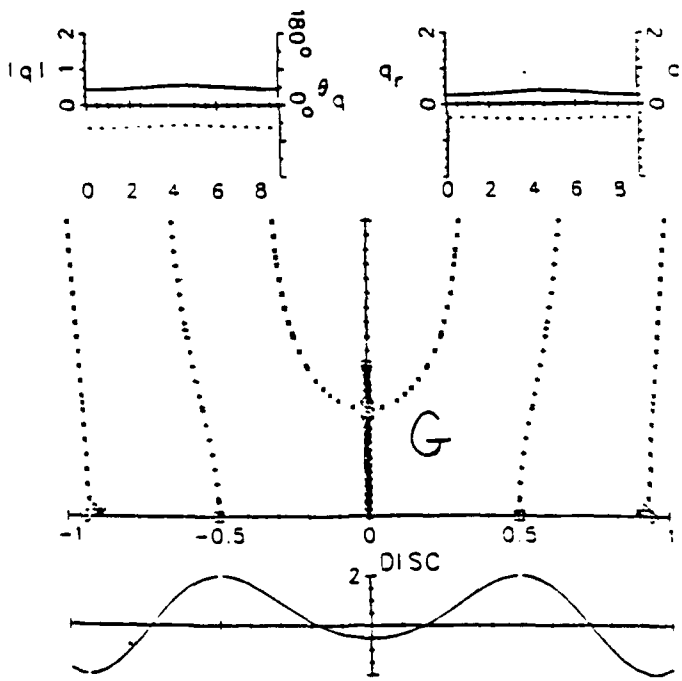

HERBST TIME = 198.

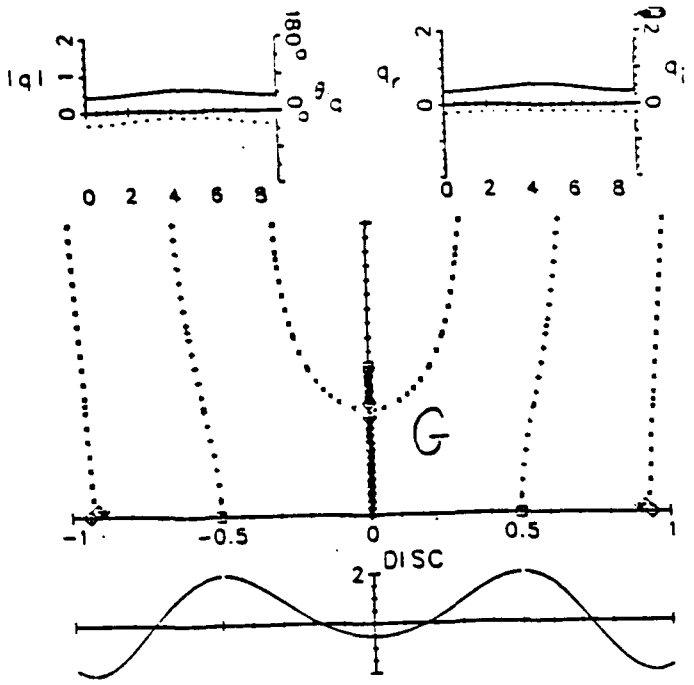

HERBST TIME = 199.5

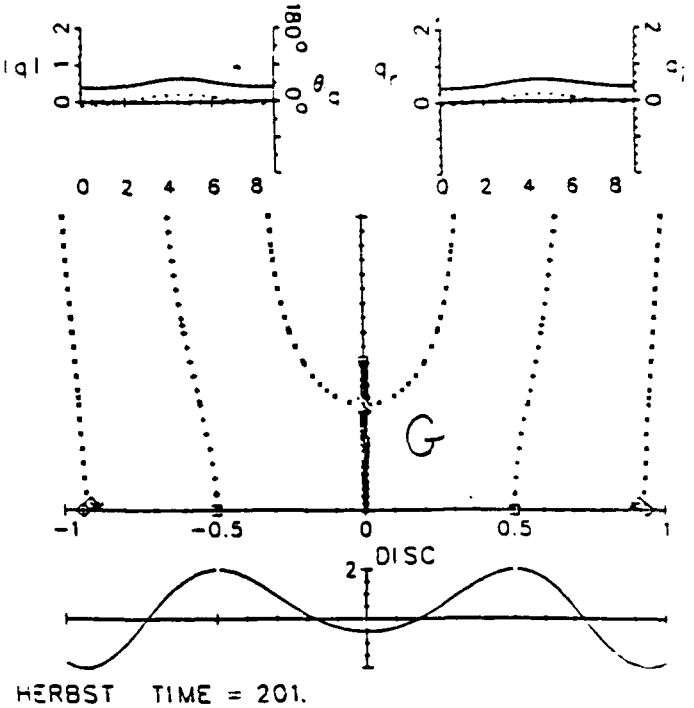

HERBST TIME = 201.

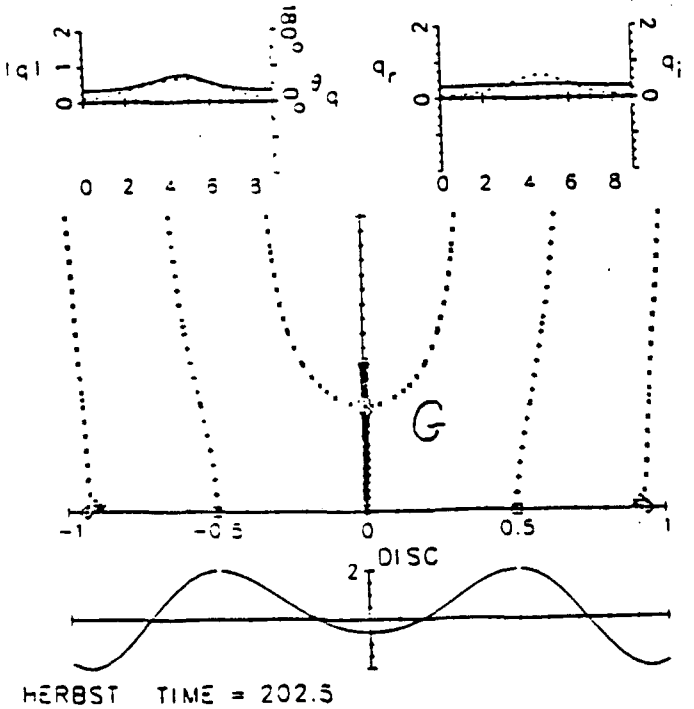

HERBST TIME = 202.5

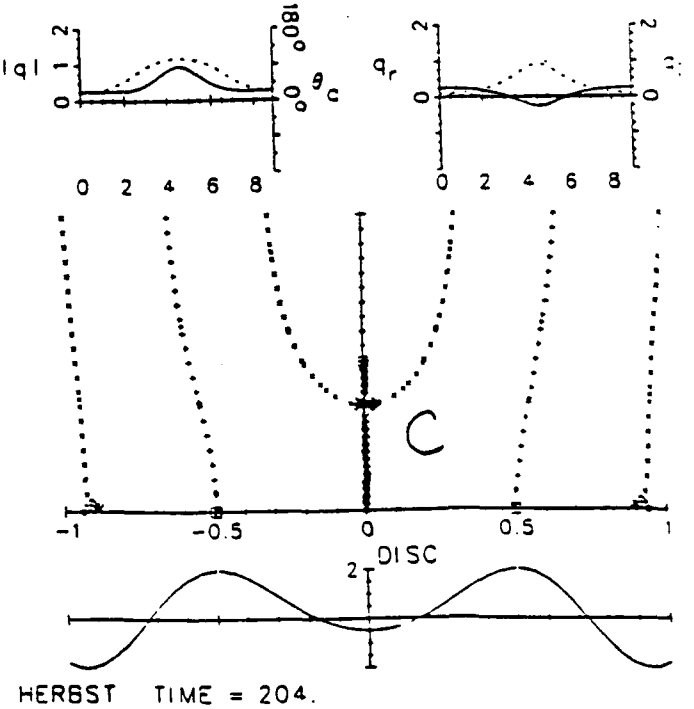

HERBST TIME = 204.

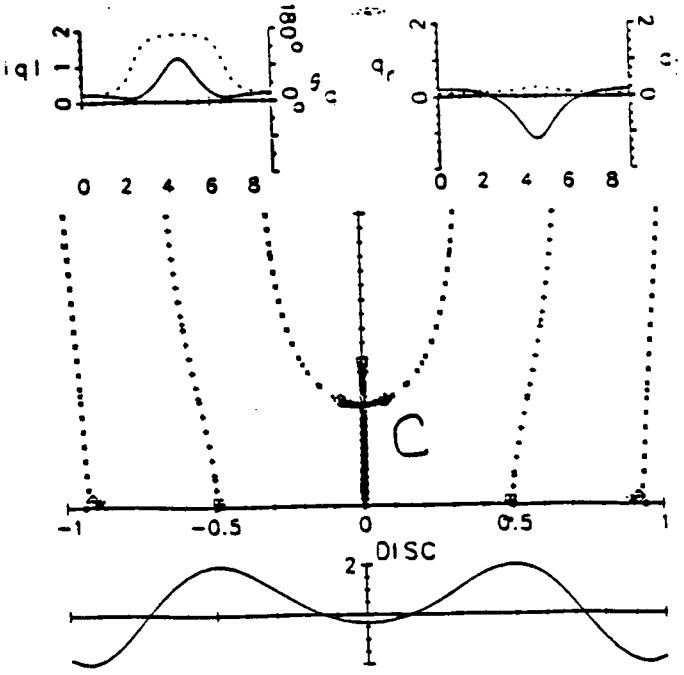

HERBST TIME = 205.5

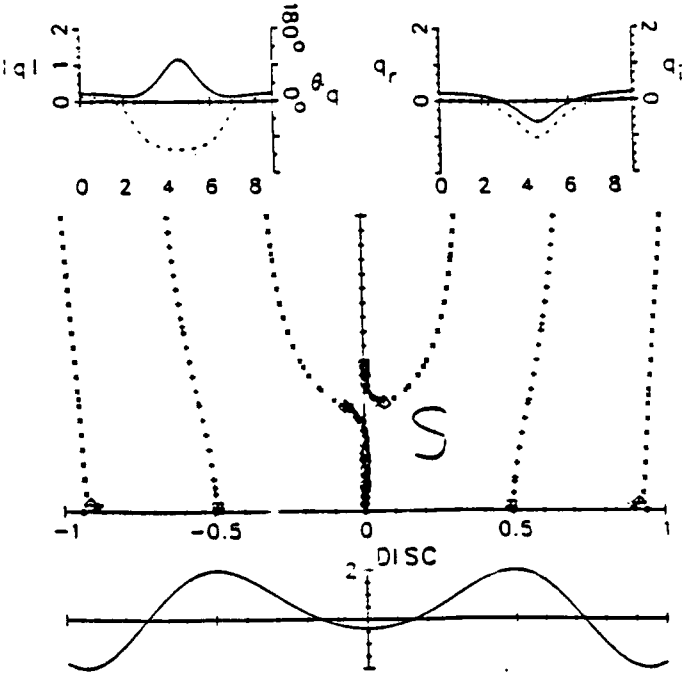

HERBST TIME = 207.

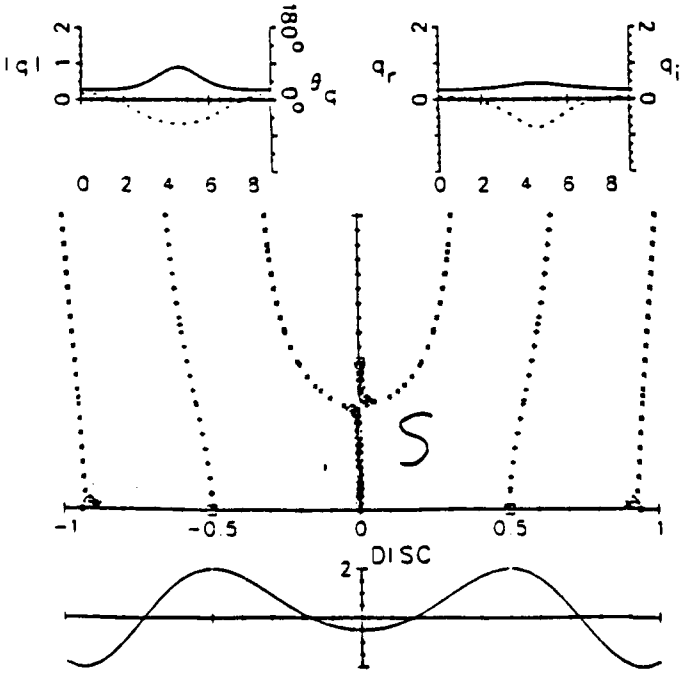

HERBST TIME = 208.5

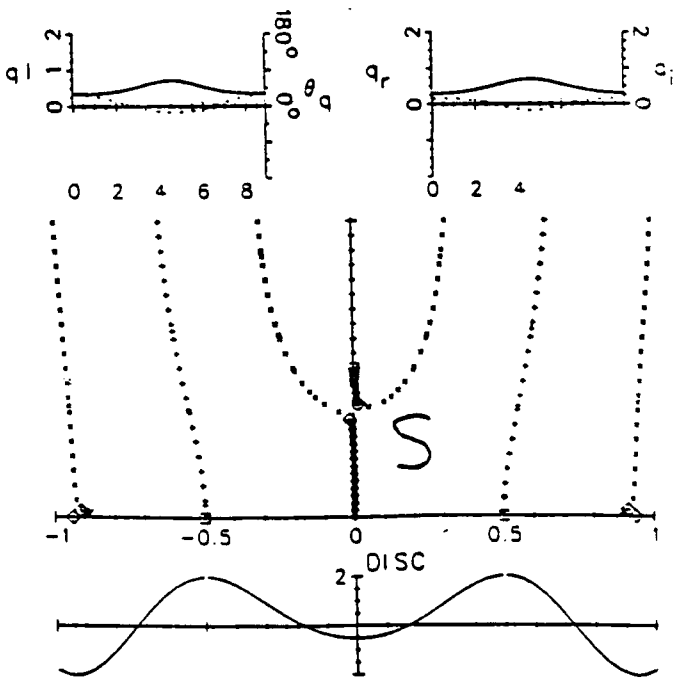

HERBST TIME = 210.